2013

Retrieval of spruce leaf chlorophyll content from airborne image data using continuum removal and radiative transfer

Zbynek Malenovsky
University of Tasmania, zbynek@uow.edu.au

Lucie Homolova
University of Zurich

Raul Zurita-Milla
University of Twente

Petr Lukes
Academy of Sciences of the Czech Republic

Veroslav Kaplan
Academy of Sciences of the Czech Republic

See next page for additional authors

Publication Details

Malenovsky, Z., Homolova, L., Zurita-Milla, R., Lukes, P., Kaplan, V., Hanus, J., Gastellu-Etchegorry, J. & Schaepman, M. E. (2013). Retrieval of spruce leaf chlorophyll content from airborne image data using continuum removal and radiative transfer. Remote Sensing of Environment: an interdisciplinary journal, 131 85-102.

Retrieval of spruce leaf chlorophyll content from airborne image data using continuum removal and radiative transfer

Abstract

We investigate combined continuum removal and radiative transfer (RT) modeling to retrieve leaf chlorophyll a & b content (Cab) from the AISA Eagle airborne imaging spectrometer data of sub-meter (0.4 m) spatial resolution. Based on coupled PROSPECT-DART RT simulations of a Norway spruce (Picea abies (L.) Karst.) stand, we propose a new Cab sensitive index located between 650 and 720 nm and termed ANCB650-720. The performance of ANCB650-720 was validated against ground-measured Cab of ten spruce crowns and compared with Cab estimated by a conventional artificial neural network (ANN) trained with continuum removed RT simulations and also by three previously published chlorophyll optical indices: normalized difference between reflectance at 925 and 710 nm (ND925&710), simple reflectance ratio between 750 and 710 nm (SR750/710) and the ratio of TCARI/OSAVI indices. Although all retrieval methods produced visually comparable Cab spatial patterns, the ground validation revealed that the ANCB650-720 and ANN retrievals are more accurate than the other three chlorophyll indices (R2 = 0.72 for both methods). ANCB650-720 estimated Cab with an RMSE = 2.27 μg cm− 2 (relative RRMSE = 4.35%) and ANN with an RMSE = 2.18 μg cm− 2 (RRMSE = 4.18%), while SR750/710 with an RMSE = 4.16 μg cm− 2 (RRMSE = 7.97%), ND925&710 with an RMSE = 9.07 μg cm− 2 (RRMSE = 17.38%) and TCARI/OSAVI with an RMSE = 12.30 μg cm− 2 (RRMSE = 23.56%). Also the systematic RMSES was lower than the unsystematic one only for the ANCB650-720 and ANN retrievals. Our results indicate that the newly proposed index can provide the same accuracy as ANN except for Cab values below 30 μg cm− 2, which are slightly overestimated (RMSE = 2.42 μg cm− 2). The computationally efficient ANCB650-720 retrieval provides accurate high spatial resolution airborne Cab maps, considerable as a suitable reference data for validating satellite-based Cab products.

Disciplines

Medicine and Health Sciences | Social and Behavioral Sciences

Publication Details

Malenovsky, Z., Homolova, L., Zurita-Milla, R., Lukes, P., Kaplan, V., Hanus, J., Gastellu-Etchegorry, J. & Schaepman, M. E. (2013). Retrieval of spruce leaf chlorophyll content from airborne image data using continuum removal and radiative transfer. Remote Sensing of Environment: an interdisciplinary journal, 131 85-102.

Authors

Zbynek Malenovsky, Lucie Homolova, Raul Zurita-Milla, Petr Lukes, Veroslav Kaplan, Jan Hanus, Jean-Philippe Gastellu-Etchegorry, and Michael E. Schaepman

Retrieval of spruce leaf chlorophyll content from airborne image data using continuum removal and radiative transfer

Zbyněk Malenovský[a,b,*], Lucie Homolová[b,c], Raúl Zurita-Milla[d], Petr Lukeš[e], Věroslav Kaplan[e], Jan Hanuš[e], Jean-Philippe Gastellu-Etchegorry[f] and Michael E. Schaepman[b]

[a] *School of Geography and Environmental Studies, University of Tasmania, Private Bag 76, 7001 Hobart, Australia*

[b] *Remote Sensing Laboratories, Department of Geography, University of Zürich, Winterthurerstrasse 190, CH-8057 Zürich, Switzerland*

[c] *Centre for Geo-Information, Wageningen University, Droevendaalsesteeg 3/PO Box 47, 6700 AA Wageningen, The Netherlands*

[d] *Department of Geo-information Processing, Faculty of Geo-Information Science and Earth Observation, University of Twente, PO Box 217, 7500 AE Enschede, The Netherlands*

[e] *Global Change Research Centre, Academy of Sciences of the Czech Republic, v.v.i., Bělidla 986/4a, 603 00 Brno, Czech Republic*

[f] *Centre d'Etudes Spatiales de la Biosphère, UPS-CNES-CNRS-IRD, 18 Avenue Edouard Belin, BPI 2801, 31401 Toulouse, Cedex 9, France*

* *Corresponding author:* Zbyněk Malenovský

School of Geography and Environmental Studies, University of Tasmania

Private Bag 76, Hobart 7001, Australia

Phone: +61 3 6226 7614

Fax: +61 3 6226 7809

Email address: zbynek.malenovsky@gmail.com

Abstract

We investigate combined continuum removal and radiative transfer (RT) modeling to retrieve leaf chlorophyll a & b content (C_{ab}) from the AISA Eagle airborne imaging spectrometer data of sub-meter (0.4 m) spatial resolution. Based on coupled PROSPECT-DART RT simulations of a Norway spruce (*Picea abies* (L.) Karst.) stand, we propose a new C_{ab} sensitive index located between 650 and 720 nm and termed $ANCB_{650-720}$. The performance of $ANCB_{650-720}$ was validated against ground-measured C_{ab} of ten spruce crowns and compared with C_{ab} estimated by a conventional artificial neural network (ANN) trained with continuum removed RT simulations and also by three previously published chlorophyll optical indices: Normalized Difference between reflectance at 925 and 710 nm ($ND_{925\&710}$), Simple reflectance Ratio between 750 and 710 nm ($SR_{750/710}$) and the ratio of TCARI/OSAVI indices. Although all retrieval methods produced visually comparable C_{ab} spatial patterns, the ground validation revealed that the $ANCB_{650-720}$ and ANN retrievals are more accurate than the other three chlorophyll indices (R^2 = 0.72 for both methods). $ANCB_{650-720}$ estimated C_{ab} with an RMSE = 2.27 μg cm^{-2} (relative RRMSE = 4.35%) and ANN with an RMSE = 2.18 μg cm^{-2} (RRMSE = 4.18%), while $SR_{750/710}$ with an RMSE = 4.16 μg cm^{-2} (RRMSE = 7.97%), $ND_{925\&710}$ with an RMSE = 9.07 μg cm^{-2} (RRMSE = 17.38%) and TCARI/OSAVI with an RMSE = 12.30 μg cm^{-2} (RRMSE = 23.56%). Also the systematic $RMSE_S$ was lower than the unsystematic one only for the $ANCB_{650-720}$ and ANN retrievals. Our results indicate that the newly proposed index can provide the same accuracy as ANN except for C_{ab} values below 30 μg cm^{-2}, which are slightly overestimated (RMSE = 2.42 μg cm^{-2}). The computationally efficient $ANCB_{650-720}$ retrieval provides accurate high spatial resolution airborne C_{ab} maps, considerable as a suitable reference data for validating satellite-based C_{ab} products.

Keywords: Chlorophyll retrieval, Imaging spectroscopy, Continuum removal, Radiative transfer, PROSPECT, DART, Optical indices, Norway spruce, High spatial resolution, AISA.

---

1. Introduction

Chlorophyll macromolecules are evolutionarily one of the most stable structures used by photosynthetically active organisms for light harvesting and energy transduction (Ustin et al., 2009). Therefore, they are playing an important role in the assimilation of carbon by green vegetation, accounting for 57 Gt of carbon per year (Normile, 2009). The total amount of chlorophyll pigments, which is reacting on surrounding environmental conditions and stress agents including anthropogenic pollutants (Buonasera et al., 2011), indicate the actual physiological status of plants (i.e. their current health and/or phenological states).

Chlorophyll molecules (mainly *a*, *b*, but also *c*, *d*, and *f*) demonstrate a strong spectral absorption in the blue and red part of the electromagnetic spectrum (Chen et al., 2010). These absorption features allow space-borne mapping of vegetation chlorophyll *a* & *b* content (C_{ab}) from high spectral resolution data acquired by spectrometers (Harris & Dash, 2010). A challenging task is, however, to validate the accuracy of satellite maps that are derived at broad spatial resolutions ranging from tens to hundreds of meters (Dash et al., 2010; Stagakis et al., 2010). Although C_{ab} is relatively stable during the high vegetation season, it changes rapidly at the beginning and at the end of the season. Therefore, traditional ground based validation of satellite maps is not only time consuming and expensive, but also potentially inaccurate due to the need of collecting many chlorophyll samples in a relatively short time. An alternative solution for spatial validation of satellite products might be the use of high spatial resolution chlorophyll maps retrieved from airborne imaging spectrometers (Moorthy et al., 2008; Zarco-Tejada et al., 2004; Zhang et al., 2008).

High spatial resolution mapping of forest C_{ab} needs to account for the spatially heterogeneous structure of the forest environment (Verrelst et al., 2010). The hierarchical canopy architecture, resulting from foliage clumping at several spatial scales (Písek et al., 2011; Smolander & Stenberg, 2003; Stenberg, 1996), and the presence of various non-photosynthetic scatterers (e.g. branches and trunks) induce strong reflectance anisotropy and high spatial variability (Malenovský et al., 2008). The confounding influence of forest structure on imaging spectrometer-based retrievals of foliar biochemistry can be minimized by combining a continuum removal method (Clark & Roush, 1984) with vegetation canopy radiative transfer (RT) modeling (Myneni, 1991).

The reflectance continuum removal transformation enhances and standardizes specific absorption features of the foliar biochemical constituents (Broge & Leblanc, 2001), in our case chlorophylls. Kokaly & Clark (1999) used normalized band depths calculated from specific continuum-removed (CR) absorption features of leaf reflectance to estimate concentrations of nitrogen, lignin, and cellulose. Curran et al. (2001) refined this methodology and employed CR band depths normalized to i) the band depth at the center of the absorption feature (abbreviated BNC) or ii) the area of the absorption feature (abbreviated BNA) to estimate C_{ab}. Underwood et al. (2003) used the CR technique for mapping invasive plant species, Kokaly et al. (2003) for discriminating different vegetation types in the Yellowstone National Park, and Schmidt & Skidmore (2003) for differentiating saltmarsh vegetation types. More recently, the CR based methods have been successfully applied to map subgenera of two Australian Eucalyptuses (Youngentob et al., 2011), or to quantify grass forage nutrients of an African savanna (Knox et al., 2011).

Three-dimensional (3D) RT models simulate photon interactions with objects within the solar reflective and/or emissive part of the electromagnetic spectrum (Kimes & Kirchner, 1982; Myneni et al., 1992). Radiative transfer of complex natural and urban landscapes is modeled using various computing techniques such as ray tracing or discrete ordinate methods (Disney et al., 2000; Gastellu-Etchegorry et al., 2004). Several 3D models were designed with an intention to simulate physically RT within forest environments of high structural complexity (Disney et al., 2006; Schaepman et al., 2009; Widlowski et al., 2006 and 2008). This ability makes them ideal to develop methods that can separate and suppress the confounding influence of forest structure on estimates of foliar biochemistry (Zarco-Tejada et al., 2001).

Several previously published studies have introduced a concept of estimating C_{ab} from airborne high spatial resolution imaging spectroscopy data with optical indices upscaled from leaf to canopy level using vegetation radiative transfer modeling (Haboudane et al., 2002; le Maire et al., 2008, Moorthy et al., 2008; Zhang et al., 2008). Following this concept, the objective of our study is to investigate the potential use of continuum removal transformation for quantitative C_{ab} mapping from airborne data of sub-meter spatial resolution. For this purpose, we use reflectance spectra of Norway spruce (*Picea abies* (L.) Karst.) crowns simulated using a coupled PROSPECT-DART leaf-canopy RT model and we propose a new continuum removal based optical index termed $ANCB_{650-720}$.

2. Material and Methods

As this study exploits several interconnected remote sensing/ground observations, laboratory analyses, and computationally intensive methods, we first describe a general synopsis of principal methodological steps shown in Fig. 1. Field measurements collected during a ground/flight campaign were used: i) to process spectral images acquired with an airborne imaging spectrometer, ii) to parameterize PROSPECT-DART radiative transfer modeling, and also iii) to produce the validation dataset (ground truth) for ten sampled spruce trees. The spectral bands simulated by the DART model allowed us to establish a statistical relationship between C_{ab} and four C_{ab} sensitive optical indices, i.e. a new optical index named Area under continuum-removed curve Normalized to the Chlorophyll absorption Band depth between 650 and 720 nm ($ANCB_{650-720}$) and three published indices: Normalized Difference between reflectance at 925 and 710 nm ($ND_{925\&710}$; le Maire et al., 2008), Simple reflectance Ratio between 750 and 710 nm ($SR_{750/710}$; Zarco-Tejada et al., 2004) and TCARI/OSAVI ratio (Haboudane et al., 2002). The RT simulations were also used to train a C_{ab} estimating artificial neural network (ANN; Bacour et al., 2006; Combal et al., 2003). C_{ab} of sunlit parts of Norway spruce crowns were estimated from geocoded, radiometrically and atmospherically corrected airborne spectral images of an AISA Eagle spectrometer by applying the following methods: i) the statistical relationships established between C_{ab} and the optical indices and ii) the properly trained ANN. The ANN results are cross-compared with estimates of the optical indices, including the newly proposed $ANCB_{650-720}$ index. Finally, the accuracy of the C_{ab} retrievals is validated with ground (laboratory) measured C_{ab}, extracted from needle samples of ten spruce tree crowns. The following subsections are further detailing each methodological step illustrated in Fig. 1.

[Fig. 1 about here.]

2.1. Experimental test site

A Norway spruce monoculture located nearby the permanent experimental eco-physiological research station Bílý Kříž in the Moravian-Silesian Beskydy Mountains (eastern part of the Czech Republic; 18.54°E, 49.50°N, altitude 936 m above sea level) was chosen as test site of this study. In 2004 the regularly spaced 26 years old spruce stand had a canopy height between 10 and 12 m, an average diameter at breast height (DBH) of about 13 cm and a leaf area index (LAI) ranging between 7 and 9 m^2 m^{-2}. The Norway spruce monoculture was subject of an intensive ground investigation characterizing spatially canopy structure, optical properties of leaves and other canopy elements, and foliar biochemistry including C_{ab}. Detailed abiotic and biotic characteristics of the Bílý Kříž study site and all ground measurement methods are described in Malenovský et al. (2008).

2.2. Processing and classification of the airborne AISA Eagle spectral images

Imaging spectroscopy data of the Bílý Kříž experimental stand was acquired under clear sky conditions by a pushbroom VNIR Airborne Imaging Spectroradiometer (AISA) Eagle (Spectral Imaging, Specim Ltd., Finland) on September 18th 2004 (around solar noon). The acquired digital numbers of 64 spectral bands between 398.39 and 983.06 nm (spectral sampling distance of about 10 nm) were transformed into radiance values using the sensor specific calibration equations in the CaliGeo software (Spectral Imaging, Specim Ltd., Finland). An empirical line atmospheric correction (Smith & Milton, 1999) and nadir image normalization was carried out using ground-measured spectra of five fabricated Lambertian calibration panels in the ATCOR-4 software (Richter & Schläpfer, 2002). The atmospherically corrected AISA Eagle images of 0.4 m spatial resolution were then geo-orthorectified into the Universal Transverse Mercator (UTM) geographic projection (zone 34 North) using a digital elevation model of 2 m vertical resolution (0.4 m horizontal spatial resolution) and the aircraft positional data recorded by the Aerocontrol IIB inertial navigation system (Ingenieur-Gesellschaft für Interfaces, IGI GmbH, Germany). A detailed description of the radiometric, atmospheric, and geometric corrections and also the accuracy of the resulting AISA Eagle hemispherical directional reflectance function (HDRF; Schaepman-Strub et al., 2006) assessed from clay bare soil, gravel road, and grass canopy spectral measurements, is available in Malenovský et al. (2008).

A subset of approximately 200 by 320 m, covering the extent of the experimental forest stand, was extracted from the AISA Eagle image mosaic. The 0.4 m spatial resolution of AISA imagery allowed the identification of individual tree crowns and differentiation of their sunlit and shaded parts using a supervised maximum likelihood classification (ENVI software; ITT Visual Information Solutions) (Fig. 2). Three optical indices sensitive to the vegetation structure (LAI): i) Normalized Difference Vegetation Index (NDVI = (R_{755}–

R_{680})/(R_{755}+R_{680}); Tucker, 1979), ii) Weighted Difference Vegetation Index (WDVI = R_{755}–1.376*R_{680}; Clevers, 1989), and iii) Simple Ratio (SR = R_{755}/R_{708}; Jordan, 1969) were computed and added to the original set of AISA spectral bands to enhance spectral differences between the ground with understory and the spruce crowns. The AISA Eagle image was at first classified into five spectrally distinguishable classes: i) sunlit tree crowns, ii) shaded tree crowns, iii) sunlit ground and understory, iv) shaded bare ground, and v) shaded understory vegetation. In the second step, a local majority filter with a moving window of 3x3 pixels was applied to remove the single misclassified pixels. Finally, classes iii), iv) and v) were merged into a general class of 'background' (Fig. 2). Five hundred validation pixels were randomly selected from nine digitized regions of interests that were evenly distributed over the forest site for an accuracy assessment purpose. Each selected pixel was visually assigned to one of the three classes and used to compute the classification confusion error matrix. An overall maximum likelihood classification accuracy of 92% (producer accuracies from 90 to 98% and user accuracies from 82 to 96%) with a Kappa coefficient of 0.864 was achieved. Similarly to Zarco-Tejada et al. (2004), we selected only sunlit crown pixels (classification accuracy of 96%) to be used in the subsequent C_{ab} estimation. The motivation for using just sunlit pixels is to include only remotely sensed HDRF of a high intensity that possess a high signal-to-noise ratio. The mean HDRF of AISA shaded crown pixels gaining about half intensity of the sunlit crown HDRF signal (Fig. 3) is likely to result in a lower C_{ab} accuracy.

[Fig. 2 about here.]

[Fig. 3 about here.]

2.3. Reflectance continuum removal and selection of the suitable spectral range

The purpose of the reflectance continuum removal transformation is to enhance and standardize the specific absorption features of the biochemical constituents (Kokaly & Clark, 1999). To achieve this, the CR spectral interval must contain wavelengths that are most sensitive to the concentration changes of the particular biochemical absorbent. Proper location and width (i.e. starting and ending wavelength) of the CR part of spectra is, therefore, crucial for the quantification of the retrieved biochemical compounds. Fig. 4 shows the mean C_{ab} specific absorption coefficients (k_{ab}) of the PROSPECT radiative transfer model for Norway spruce needles (Malenovský et al., 2006) with a distinct absorption feature between 550 and 750 nm caused by the electron transition of the photosynthetic processes (Curran, 1989). According to Gitelson et al. (1996), the red edge wavelengths most sensitive to C_{ab} are located between 690 and 710 nm. The C_{ab} absorption is strongly influencing the shorter wavelengths of the red edge region, while the longer wavelengths are driven by canopy structural characteristics like leaf area index (LAI) and leaf angle distribution (LAD) (Liu et al., 2004). To include the most sensitive C_{ab} absorption wavelengths and to avoid in the same time negative interferences of the canopy structure, we decided to start the continuum removal interval in the middle of the red chlorophyll absorption feature (550 – 750 nm), i.e. at the wavelength of 650 nm, and to end it in the middle of the red edge region between 680 and 760 nm, i.e. at the wavelength of 720 nm (see Fig. 4). The forest RT modeling (section 2.4) was, therefore, restricted to simulate only the AISA Eagle spectral bands located in the spectral region between 650 and 720 nm.

[Fig. 4 about here.]

2.4. PROSPECT-DART radiative transfer modeling

The leaf optical properties were simulated using the PROSPECT leaf RT model (version 3) (Jacquemoud & Baret, 1990), adjusted for Norway spruce needles by Malenovský et al. (2006). They were upscaled to the level of forest canopy with Discrete Anisotropic Radiative Transfer (DART; Gastellu-Etchegorry et al., 1996); a 3D RT model developed in CESBIO (Center for the Study of the Biosphere from Space, UPS-CNRS-CNES-IRD, France). A detailed description of specific DART functions and input parameters required to perform an ecologically sound 3D radiative transfer of a representative Norway spruce stand is provided in Malenovský et al. (2008). Herein we summarize only the most important aspects of our RT modeling that resulted in a database of simulated airborne spectral images. We subsequently use the term Look-Up-Table (LUT) for these simulated data.

Input parameters of our RT modeling were derived from the field measurements collected at the Bílý Kříž test site during a join flight/field campaign in 2004 and destructive tree sampling performed in the previous years (Pokorný & Marek, 2000). Table 1 summarizes the key fixed and varied input parameters required to build a representative virtual 3D spruce forest stand. The number of tree crowns in a simulated scene varied according to the desired canopy cover (CC) of two predefined tree distributions as follows: i) four (CC = 75%), five (CC = 85%), and six (CC = 95%) trees in case of a regular tree distribution, and ii) five (CC = 75%), six (CC = 85%), and seven (CC = 95%) trees in case of an irregular (clumped) tree distribution. Also, the LAI of the simulated stands was kept as a free variable, varying in accordance with ground measurements between 4 and 9 $m^2 m^{-2}$ with a step of 1 $m^2 m^{-2}$. Crowns with heights from 9 to 11 meters were constructed out of 11 horizontal levels of foliage turbid cells, characterized by the specific leaf average angle ranging from 25° to 40°. The vertical and horizontal foliage distributions within a crown, the trunk parameters, geometry of branches of the first order, and the distribution of fine woody twigs were adjusted according to destructive field measurements (for detailed description see Malenovský et al., 2008). The forest stand background, covering a continuous slope of 13.5°, was modeled as a mixture of bare soil and senescent needle litter.

[Table 1 about here.]

The directional-hemispherical optical properties of the scene surfaces (i.e. bark of trunks and branches, forest litter and soil) were defined in DART as being of a Lambertian nature.

Several samples of these surfaces were collected during fieldwork and their reflectance was measured in laboratory using an optical integrating sphere Li-1800-12 (Li-Cor, Inc., USA) coupled with a FieldSpec PRO spectroradiometer (ASD, Inc., USA) according to the standard Li-Cor sphere measurement protocol. The optical properties (i.e. directional-hemispherical reflectance and transmittance) of the three spruce needle age-classes: i) needles of the current growing season (C), ii) needles of the previous growing season (C+1), and iii) needles older than the previous growing season (C++) were also measured in the Li-1800-12 integrating sphere according to the protocol developed and described in Malenovský et al. (2006). These measurements were used to adjust the PROSPECT model for three age-classes of sunlit and shaded spruce needles (Malenovský et al., 2006) and consequently used to retrieve the PROSPECT mesophyll structure parameter ~ N (Table 2) according to the method described in Jacquemoud et al. (1996). Needle optical properties entering the DART simulations were obtained from the adjusted PROSPECT model parameterized with the inputs summarized in Table 2. The retrieved variable of interest (C_{ab}) was kept free, ranging between the lowest (10 $\mu g\ cm^{-2}$) and the highest (100 $\mu g\ cm^{-2}$) value with an increment of 10 $\mu g\ cm^{-2}$, while leaf mass per area ~ C_m, water content ~ C_w and optical structural parameter N were fixed based on the needle sample laboratory measurements. Further details on leaf biochemistry measurements are provided in section 2.6.

[Table 2 about here.]

All combinations of free PROSPECT-DART input parameters (i.e. two tree distributions, three CC, six LAIs, and ten C_{ab} values) resulted in 360 simulations of Bidirectional Reflectance Factor (BRF) images containing eight AISA Eagle spectral bands between 650 and 720 nm (Table 1). Since the DART discrete ordinate RT simulations were performed without specifying the atmosphere between the stand canopy and the airborne sensor, the resulting top of canopy BRF values are comparable with the atmospherically corrected AISA

Eagle spruce canopy reflectance images. The maximum likelihood classification method was applied once again on the PROSPECT-DART simulated spectral images to separate sunlit crown parts from shaded and from forest background pixels. After that, the BRFs of sunlit crown pixels of each simulated scene were averaged, continuum-removed, and stored together with the corresponding RT input parameters in the LUT.

2.5. Retrieval of leaf chlorophyll content using optical indices and artificial neural network

We implemented and cross-compared five retrieval approaches estimating forest canopy C_{ab} from the airborne spectral AISA Eagle images using the PROSPECT-DART simulated LUT. The first approach employed the newly designed optical index $ANCB_{650-720}$, defined as the Area Under Curve of CR reflectance between 650 and 720 nm ($AUC_{650-720}$) normalized by the CR Band Depth at 670 nm (CBD_{670}). The $AUC_{650-720}$ was calculated according to the following equation:

$$\mathrm{AUC}_{650\text{-}720} = \frac{1}{2}\sum_{j=1}^{n-1}\left(\lambda_{j+1} - \lambda_j\right)\left(\rho_{j+1} + \rho_j\right), \quad (1)$$

where ρ_j and ρ_{j+1} are values of the CR reflectance at the *j* and *j*+1 bands, λ_j and λ_{j+1} are wavelengths of the *j* and *j*+1 bands, and *n* is the number of used spectral bands. The results of three C_{ab} sensitive optical indices that have been used in the RT upscaling scheme in previous studies were additionally analyzed and compared with the $ANCB_{650-720}$ outcomes. The Normalized Difference optical index ($ND_{925\&710}$), computed between reflectance at 925 (ρ_{925}) and 710 (ρ_{710}) nm as:

$$ND_{925\&710} = (\rho_{925} - \rho_{710}) / (\rho_{925} + \rho_{710}), \quad (2)$$

was recommended as the best performing index for the C_{ab} retrieval of small broadleaf canopies from Hyperion satellite data by le Maire et al. (2008). The Simple reflectance Ratio index ($SR_{750/710}$), computed as the red edge spectral transform:

$$SR_{750/710} = \rho_{750} / \rho_{710}\,, \tag{3}$$

where ρ_{750} and ρ_{710} is reflectance at 750 and 710 nm, respectively, was upscaled for C_{ab} estimation of Jack pine (*Pinus banksiana* Lamb.) stands using the PROSPECT and SPRINT RT models by Zarco-Tejada et al. (2004). Finally, Haboudane et al. (2002) proposed the ratio of TCARI and OSAVI optical indices as a LAI and soil background independent C_{ab} proxy for agricultural crops. The index is computed as the ratio of:

$$\mathrm{TCARI} = 3\left[\left(\rho_{700} - \rho_{670}\right) - 0.2\left(\rho_{700} - \rho_{550}\right)\left(\frac{\rho_{700}}{\rho_{670}}\right)\right] \tag{4}$$

and

$$\mathrm{OSAVI} = \frac{\left(1 + 0.16\right)\left(\rho_{800} - \rho_{670}\right)}{\left(\rho_{800} + \rho_{670} + 0.16\right)}\,, \tag{5}$$

where $\rho_{550,}$ $\rho_{670,}$ ρ_{700} and ρ_{800} are the reflectance values at 550, 670, 700 and 800 nm. Recently, Zhang et al. (2008) applied TCARI/OSAVI upscaled by the PROSPECT and 4-SCALE RT models on Compact Airborne Spectrographic Imager (CASI) data to map C_{ab} of Black spruce (*Picea mariana* Mill.) stands in Canada. All four optical indices were computed for each PROSPECT-DART simulation and stored in our LUT. The empirical functions describing the closest relationship between the index values and the simulated C_{ab} were fitted in the PeakFit software package (Systat Software, Inc., USA). The best fitting equations (with the highest coefficient of determination R^2, significant at a given probability level *p*) were then applied per-pixel to the AISA Eagle imagery to estimate C_{ab} of the sunlit crown pixels.

Apart from optical indices, the ANN based retrieval approach has been successfully employed in LUT inversions of RT models (Bacour et al., 2006; Combal et al., 2003). Therefore, we decided to cross-compare the results of the optical indices with estimates from the computationally different ANN approach. After testing several ANN architectures in the MATLAB neural network toolbox (The MathWorks, Inc., USA), we chose a two-layer feed-forward back-propagation ANN. The first (input) layer was composed out of six neurons corresponding to the six simulated CR AISA Eagle wavebands and associated with a tan-sigmoidal transfer function. A linear transfer function was assigned to the second (output) layer that contained only one neuron producing the C_{ab} estimate. Half of the PROSPECT-DART simulated LUT entries were randomly selected to train the predefined ANN. To avoid a scaling factor problem (each wavelength has a typical range of values) and to increase the convergence performance of the training procedure, the ANN inputs and outputs were standardized. Each input/output had a mean value of zero and standard deviation of one. The high-speed processing Levenberg-Marquardt optimization algorithm was applied for the network training. To prevent a potential over-training, an early stopping technique was implemented using a quarter of the randomly selected PROSPECT-DART LUT entries. Finally, the performance of the ANN was tested with the remaining quarter of the LUT entries. In particular, the root mean square error (RMSE) and the coefficient of determination R^2 were computed to test the ANN performance. The best performing ANN (i.e. not over-fitted and with the lowest possible RMSE and an R^2 close to one) was employed to retrieve C_{ab} from the AISA Eagle sunlit crown pixels.

To investigate the relationship of $ANCB_{650-720}$ and the three other optical indices with C_{ab} also in a case of broadleaf canopies, we performed additional PROSPECT-DART simulations for a virtual 1D homogeneous turbid medium of grassland and for a structurally more complex 3D canopy of a deciduous forest stand. The methodology and results of this RT exercise are provided in Appendix A. In Appendix B we demonstrate differences in the statistical dependency of $ANCB_{650-720}$ on C_{ab} when established for sunlit or shaded pixels of Norway spruce crowns by RT models.

2.6. Validation of leaf chlorophyll content estimates using ground truth measurements

Ten individual spruce trees were randomly selected in a transect crossing the experimental forest stand from East to West for the validation of the airborne C_{ab} maps (Fig 2a). The transect direction was following the terrain elevation gradient in expectation to capture a variability in C_{ab} due to the increasing environmental stress at higher altitude. The sampled crowns were localized with a decimeter accuracy using a DGPS device combined with the Field-Map system composed of laser telemeter, digital compass, and forest ecosystem mapping software (Institute of Forest Ecosystem Research, IFER Ltd., Czech Republic). Sampling took place in five days following the AISA Eagle acquisition date. Shoots of the three most recent age-classes were collected from a sun-exposed branch of the 3rd whorl (counted from top of the crown) and from a shaded branch (below 10th whorl) of each crown. Depending on their size, approximately twenty needles were randomly detached from each sampled shoot. Half of them were fresh-weighted, and scanned for a later calculation of their leaf hemisurface area according to the method described by Homolová et al. (2012). The second half was frozen in liquid nitrogen, closed in a cooled dark container, and transported to the laboratory for a destructive C_{ab} analysis.

The laboratory C_{ab} measurements were carried out according to the standardized protocol established and verified in previous studies (Lhotáková, et al., 2007; Malenovský et al., 2006). On average, 0.5 g of the sampled frozen needles were bleached in 10 ml dimethylformamide (DMF), while keeping them in the dark and at 8° C for five consecutive days (Porra et al., 1989). The absorbance of the extracts was measured at wavelengths of 480, 647, and 664 nm using a Unicam Helios α spectrophotometer (Unicam Ltd., Cambridge, UK). A complementary needle sample was oven-dried at 60°C for 48 hours and weighted to obtain the sample dry matter content. Leaf chlorophyll *a* & *b* concentrations in mg g^{-1} of dry matter were calculated according to the equations of Wellburn (1994). They were transformed in μg cm^{-2} using the measured specific leaf area (SLA), defined as the ratio of the hemisurface leaf area (cm^2) to the sample dry matter weight (g), according to Homolová et al. (2012).

The crown representative C_{ab} value was computed as a weighted average of six needle samples (i.e. more than 10 needles of three age-classes collected from the 3rd and below the 10th whorl). Two types of measurements were collected to determine the weights: i) the biomass of each needle age-class within the vertical crown profile (i.e. percentage of the total age-class specific needle area per vertical crown level measured destructively in 2007 from six branches) and ii) the light extinction within the vertical crown profile measured with a CANFIB optical system (Global Change Research Centre AS CR, Czech Republic; Urban et al. 2007). CANFIB consists of several light diffusers installed within a vertical crown profile and measuring the total incoming photosynthetically active radiation (PAR ~ radiation between 400 and 700 nm). The acquired relative PAR measurements expressing a fraction of the above canopy PAR per monitored crown level were coupled with the needle age-class biomass of each sampled branch to create the average weights of each branch type and needle age-class (Table 3). Finally, the sampled trees were identified in the AISA Eagle image using their GPS locations. Their sunlit crown parts (between 15 and 25 pixels representing an area of 2.4 – 4.0 m^2 each) were manually selected (see their mean AISA HDRF in Fig. 3) and their corresponding retrieved C_{ab} estimates were averaged and compared with the ground-measured dataset.

[Table 3 about here.]

2.7. Statistical analyses assessing the accuracy of chlorophyll content estimates

To assess the performance of the trained ANN and the optical indices, we computed the following statistical indicators for the retrieved and the ground-measured C_{ab}: the coefficient of determination (R^2) of a linear function, the root mean square error (RMSE) including its systematic ($RMSE_s$) and unsystematic ($RMSE_u$) components, the relative RMSE (RRMSE; computed as RMSE normalized by the C_{ab} ground measured range) and the index of agreement (*d*). Additionally, the ANN C_{ab} estimates obtained for sunlit crown pixels of the AISA Eagle image were cross-compared with the $ANCB_{650-720}$, $ND_{925\&710}$, $SR_{750/710}$ and TCARI/OSAVI estimates.

Assuming a one-to-one linear relationship between the number (N) of error free observations (O) and predictions (P), the RMSE of estimates and its systematic and unsystematic components can be calculated as follows (Willmott, 1981):

$$\mathrm{RMSE} = \sqrt{\sum_{i=1}^{N}\left(P_i - O_i\right)^2 \Big/ N}\,, \tag{6}$$

$$\mathrm{RMSE}_s = \sqrt{\sum_{i=1}^{N}\left(\hat{P}_i - O_i\right)^2 \Big/ N} \quad \text{and} \tag{7}$$

$$\mathrm{RMSE}_u = \sqrt{\sum_{i=1}^{N}\left(P_i - \hat{P}_i\right)^2 \Big/ N}\,, \tag{8}$$

where $\hat{P}_i = a + bO_i$, and *a* and *b* are the coefficients of an ordinary least squares regression between O and P. Both RMSE components are related to the RMSE through the following equation:

$$\mathrm{RMSE}^2 = \mathrm{RMSE}_s^2 + \mathrm{RMSE}_u^2\,. \tag{9}$$

These components offer complementary information to that of RMSE (and R^2) as they allow a deeper evaluation of the retrieval methods. If $RMSE_s$ prevails over $RMSE_u$, one can say that the retrieval method is affected by systematic errors and that it will yield biased C_{ab} estimations. On the contrary, if the RMSE is composed mostly by $RMSE_u$, then the retrieval method is as good as it can be. The index of agreement *d* complements information contained in RMSE, $RMSE_s$ and $RMSE_u$. It is expressed as:

$$d = 1 - \left(\sum_{i=1}^{N} (P_i - O_i)^2 \Big/ \sum_{i=1}^{N} \left(|'P_i| - |'O_i| \right)^2 \right), \tag{10}$$

where $'P_i = P_i - \bar{O}$ and $'O_i = O_i - \bar{O}$. The index specifies the degree to which the observed deviations of the mean observations $\bar{O}$ correspond, both in magnitude and sign, to the predicted deviations of $\bar{O}$. It is a dimensionless indicator, where d = 1.0 indicates perfect agreement between the observed and estimated observations, and d = 0.0 connotes complete disagreement. A detailed description of $RMSE_s$, $RMSE_u$ and the index of agreement is provided in Willmott (1981).

3. Results and discussion

3.1. Sensitivity of CR crown reflectance to C_{ab} and LAI

The CR bidirectional reflectance factors (BRFs) of the sunlit spruce crowns simulated between 650 and 720 nm in the coupled PROSPECT-DART model were plotted per C_{ab} level against the LAI values to investigate their sensitivity to both variables. Fig. 5 illustrates that all CR BRFs of the simulated AISA Eagle bands are insensitive to LAI changes between 4 and 9 m m^{-2}. Some sensitivity is observed for LAI values below six, where the BRF of spruce canopies is influenced by reflectance of photosynthetically inactive surfaces (woody elements) (Malenovský et al., 2008). Fig. 5 also indicates that the most C_{ab} sensitive CR BRFs of the simulated AISA Eagle bands are located at 698.72 and 708.07 nm. The wavelengths between 650 and 690 nm are only sensitive to lower C_{ab} values, mostly below 40 μg cm^{-2}, and they become saturated with increasing C_{ab}, as previously shown by Daughtry et al. (2000). Consistently with Gitelson et al. (2003, 2006), our findings show that the most suitable (sensitive) wavelengths for C_{ab} estimation are located around 710 nm (i.e. spectral interval 700 – 720 nm). Since the CR BRFs between 660 and 680 nm are rather stable and insensitive to moderate and high C_{ab}, they can be used as a normalization element of a continuum removal based C_{ab} estimator. Still, one has to keep in mind that such an estimator will retrieve the low C_{ab} estimates (≤ 25 μg cm^{-2}) with a certain systematic error.

[Fig. 5 about here.]

3.2. Design of a continuum removal based C_{ab} optical index

Fig. 6a shows that the area integrated under the simulated CR BRF curves of sunlit tree crowns between 650 and 720 nm ($AUC_{650\text{-}720}$) is exponentially related to C_{ab}. Nevertheless, due to the early saturation this exponential relationship cannot be exploited to estimate C_{ab} values above 40 μg cm^{-2} (e.g. $AUC_{650\text{-}720}$ equal to 30 corresponds with any C_{ab} from 55 up to 85 μg cm^{-2} depending on the actual LAI). Fig. 6b indicates that the CR band depth of the strongest chlorophyll absorption between 660 and 680 nm, represented in our case by the CR band depth at 670 nm (CBD_{670}), is also insensitive to C_{ab} above 40 μg cm^{-2}, but the ratio of both variables $AUC_{650\text{-}720}/CBD_{670}$ exhibits a strong near-linear (exponential) relation to C_{ab} (Fig. 6c). This new optical index, which we call 'Area under continuum-removed curve Normalized to the Chlorophyll absorption Band depth between 650 and 720 nm' ($ANCB_{650\text{-}}$

$_{720}$), can estimate C_{ab} of sunlit Norway spruce crowns independently from the LAI variation via the equation ($R^2 = 0.99$, $p < 0.001$):

$$\ln(C_{ab}) = 7.3903-7984.0135/(ANCB_{650\text{-}720})^2. \quad (11)$$

Notice in Fig. 6c how $ANCB_{650\text{-}720}$ simulated with different LAI values concentrate for each C_{ab} value into one 'narrow' (almost a single) point. This means, that for instance an $ANCB_{650\text{-}720}$ value around 48.4 will always predict a C_{ab} of 55 μg cm^{-2} regardless the variation in actual forest stand LAI and canopy closure (CC).

[Fig. 6 about here.]

Similar results were obtained also for other PROSPECT-DART simulated broadleaf canopies, i.e. homogeneous grassland and structurally heterogeneous deciduous forest stand (results in Appendix A). The $ANCB_{650\text{-}720}$ of both broadleaf canopies is linearly dependent on C_{ab} ($R^2 = 0.95$ for grassland and $R^2 = 0.99$ for deciduous forest) and it maintains its LAI independency for C_{ab} estimates higher than 30 μg cm^{-2} (Fig. A2c and A3c). A limited ability to retrieve C_{ab} below this threshold is due to spectral influence of the simulated background (bare soil), and in case of the grass canopy also due to the six leaf angle distributions (Table A1), both controlling the BRF continuum when C_{ab} absorption is too low. Because $ANCB_{650\text{-}720}$ is designed to exploit the variation in the CR reflectance due to changes in chlorophyll absorption between 650 and 720 nm, it should only be applied to pixels of pure vegetation canopy with a strong reflectance signal, i.e. in our case sunlit pixels of tree crowns. A comprehensive and systematic sensitivity analysis of $ANCB_{650\text{-}720}$ to mixed spectral information of different signal-to-noise ratios falls outside the scope of this study, but results in Appendix A suggest that an application of $ANCB_{650\text{-}720}$ to BRFs of canopies with a low LAI and C_{ab} (i.e. with a strong signal contribution from background bare soil) will result in unreliable C_{ab} estimates. Also a significant presence of non-photosynthetic surfaces (e.g. tree trunks or manmade objects) or a high noise, which distorts the shape of the chlorophyll absorption feature between 650 and 720 nm, lead logically to an erroneous C_{ab} estimate. Although the analysis of the PROSPECT-DART simulated $ANCB_{650-720}$ for shaded crown parts revealed a similar empirical relationship with C_{ab} as for sunlit crowns (Appendix B), the bottleneck for including the shaded pixels in the C_{ab} estimation is their low and spatially varying reflectance intensity and also an occasional noise in acquired airborne spectral data. Even though Fig. 3 indicates acceptable radiometric quality of the AISA shaded crown pixels, our attempt to apply the C_{ab} retrieval in those pixels resulted in estimates of a random spatial variability (results not shown). We therefore deduce, that our shaded pixels are not suitable for the C_{ab} estimation due to the limited reflectance dynamic range and the locally specific shade intensity depending on recombination of various structural and geometrical forest stand parameters (e.g. foliar density, crown shape, tree height, slope, terrain configuration, etc.).

3.3. Chlorophyll estimation using optical indices and ANN

Three additional C_{ab} sensitive optical indices were computed from the PROSPECT-DART simulated LUT according to Eq. (2), (3), (4) and (5) and related statistically to the predefined C_{ab} classes (Fig. 6def). The equation describing most accurately the dependency of $ND_{925\&710}$ on C_{ab} is a second order polynomial function ($R^2 = 0.92$, $p < 0.01$):

$$C_{ab} = 524.86(ND_{925\&710})^2 - 364.33(ND_{925\&710}) + 70.11. \quad (12)$$

$SR_{750/710}$ was related to C_{ab} linearly ($R^2 = 0.95$, $p < 0.01$) according to the following equation:

$$C_{ab} = 24.93(SR_{750/710}) - 36.38 \quad (13)$$

and TCARI/OSAVI can be used to retrieve C_{ab} through the following natural logarithm (R^2 = 0.99, $p < 0.001$):

$$C_{ab} = -56.01 \ln(\mathrm{TCARI/OSAVI}) - 53.43. \quad (14)$$

All three relationships are statistically significant, but only TCARI/OSAVI gains a variability that ensures a unique C_{ab} estimation for almost all the simulated LAI and CC combinations (Fig. 6f). The variability of $ND_{925\&710}$ and $SR_{750/710}$ is quite high, which means that a given index value can correspond with up to four possible C_{ab} estimates (Fig. 6de), depending on LAI and CC. The ANN was trained using continuum-removed AISA Eagle spectral bands of sunlit spruce crowns simulated with PROSPECT-DART models as described in section 2.5. The accuracy assessment of the trained ANN revealed that it could estimate the simulated C_{ab} values with an RMSE of 0.40 μg cm^{-2} and with an R^2 of 0.99. The ANN and the empirical functions of optical indices stated in Eq. (11), (12), (13) and (14) were consequently applied on the atmospherically corrected CR AISA Eagle spectral bands to retrieve C_{ab} of sunlit spruce crowns under investigation.

Fig. 7 shows the C_{ab} maps and relative histograms of the ANN and $ANCB_{650-720}$ retrievals and also their reciprocal difference. Fig. 7a and Fig. 7b demonstrate that the spatial pattern of both C_{ab} maps is similar, showing a large patch of low C_{ab} values at the highest elevation point of the study site (eastwards of the ecological station facility), which is exposed to a stronger environmental stress impact due to the weather conditions. C_{ab} maps produced by the $ND_{925\&710}$, $SR_{750/710}$ and TCARI/OSAVI empirical functions are having visually similar patterns (maps not shown), but their dynamic ranges and histogram distributions are shifted towards lower C_{ab} in case of $ND_{925\&710}$ and $SR_{750/710}$ or higher C_{ab} in case of TCARI/OSAVI (Fig. 8abc). We found that the lowest and the highest ANN C_{ab} estimates are equal to 14.7 μg cm^{-2} and 65.5 μg cm^{-2}, respectively, which match well with the values yielded by ANCB$_{650-720}$ (the lowest C_{ab} = 18.6 μg cm^{-2} and the highest C_{ab} = 66.9 μg cm^{-2}), but do not correspond so well with the estimates of the other three indices. For ANN and ANCB$_{650-720}$, the most frequent C_{ab} estimates are ranging between 40.0 and 44.9 μg cm^{-2} (Fig. 7de), while for ND$_{925\&710}$ they range between 30.0 and 34.9 μg cm^{-2}, for SR$_{750/710}$ between 35.0 and 39.9 μg cm^{-2}, and for TCARI/OSAVI between 50.0 and 54.9 μg cm^{-2} (Fig. 8abc). The subtraction of the ANN C_{ab} map from the ANCB$_{650-720}$ C_{ab} map revealed an absolute mean difference of only 1.8 μg cm^{-2}, with the highest prediction differences (≥ 5.0 μg cm^{-2}) appearing at the locations of low C_{ab} estimates (Fig. 7c). The mean differences between ANN and the other three indices are higher, i.e. –9.01 μg cm^{-2} for ND$_{925\&710}$, –4.30 μg cm^{-2} for SR$_{750/710}$, and 13.29 μg cm^{-2} for TCARI/OSAVI. The histogram of the ANCB$_{650-720}$–ANN C_{ab} difference shows a nearly symmetrical Gaussian distribution, with slightly higher frequencies for positive C_{ab} differences indicating a minor overestimation of ANCB$_{650-720}$ (Fig. 7f). Almost 40% of the C_{ab} estimates produced by both methods are equal and about 40% are differing by only ± 2.0 μg cm^{-2}. Differences greater than ± 2.0 μg cm^{-2} are found for less than 20% of all the examined pixels (n = 151984). The histograms of the ND$_{925\&710}$–ANN and SR$_{750/710}$–ANN C_{ab} differences are also symmetrical, but shifted significantly towards negative values, which suggests a systematic underestimation of both indices. Contrary to this, the TCARI/OSAVI–ANN histogram shows a strong shift towards higher C_{ab} values, i.e. an overestimation of C_{ab} retrieved by the index. These results demonstrate that, unlike the reflectance ratio based optical indices, both continuum removal based methods (ANN and ANCB$_{650-720}$) produce consistent estimates.

[Fig. 7 about here.]

[Fig. 8 about here.]

A per-pixel statistical comparison of the ANN with the optical indices provided in Table 4a confirms a similar performance of the ANN and $ANCB_{650-720}$ methods (R^2 = 0.85, d = 0.95). The next two highest agreements are found between ANN and $SR_{750/710}$ (R^2 = 0.52, d = 0.75), and ANN and $ND_{925\&710}$ (R^2 = 0.51, d = 0.60), while TCARI/OSAVI seems to disagree with more than half of the ANN predictions (R^2 = 0.35, d = 0.45). The $ANCB_{650-720}$ results for C_{ab} values smaller than 30 μg cm^{-2} yield, however, systematically higher values than the ANN results (Fig. 9d). This discrepancy can be attributed to the normalization of the index by the CBD_{670} term, which is not constant across the whole C_{ab} dynamic range, but slightly decreasing for C_{ab} values lower than 30 μg cm^{-2} (see Figs. 5b and 6b). Fig. 9abc illustrates a greater mismatch between the ANN method and the remaining three ratio indices, with $ND_{925\&710}$ and $SR_{750/710}$ predicting in general lower and TCARI/OSAVI generating for most of the pixels higher C_{ab} estimates.

[Table 4. about here.]

[Fig. 9 about here.]

3.4. Comparison of airborne C_{ab} estimates with ground measurements

Needle samples of ten spruce crowns were collected during the flight campaign to generate the C_{ab} ground truth as described in section 2.6. Unfortunately one of the sampled crowns had to be excluded from the original validation dataset due to the presence of a metallic meteorological tower standing next to the tree. Photons reflected from the metallic tower affected negatively the HDRF of the sampled spruce crown, which resulted in a systematic C_{ab} overestimation of about 17 μg cm^{-2} (results not shown).

The comparison of the C_{ab} values retrieved by all five estimation methods with the ground-measured C_{ab} of the nine remaining crowns is displayed in Fig. 10. Indicators assessing statistical accuracy of all the prediction methods are available in Table 4b. The highest R^2 of

0.72 with the lowest RMSE indication and *d* of approximately 0.9 were obtained for ANN and $ANCB_{650\text{-}720}$. Both approaches resulted in virtually identical RMSE values of 2.18 μg cm^{-2} for the ANN (RRMSE of 4.18%) and 2.27 μg cm^{-2} for the $ANCB_{650\text{-}720}$ (RRMSE of 4.35%) retrieval (Fig. 10ab), with $RMSE_u$ higher than $RMSE_s$. The two RMSE components are for $ANCB_{650\text{-}720}$ almost equal, while $RMSE_u$ for ANN is about two times higher than $RMSE_s$, indicating an absence of systematic errors and a prevailing presence of random errors. The opposite situation is found for the other optical indices, with $RMSE_u$ being two to almost four times lower than $RMSE_s$. The second most accurate retrieval was performed with $SR_{750/710}$ (R^2 = 0.71, d = 0.75) (Fig. 10e), followed by $ND_{925\&710}$ (R^2 = 0.64, d = 0.53) (Fig. 10d), both underestimating C_{ab} by 4.16 and 9.07 μg cm^{-2}, respectively (RRMSE of 7.97 and 17.38%). The least accurate method is the TCARI/OSAVI estimation (R^2 = 0.41, d = 0.42) with an RMSE equal to 12.30 μg cm^{-2} (RRMSE of 23.56%) (Fig. 10f). A visual investigation of the C_{ab} map revealed that the systematic overestimation of the TCARI/OSAVI retrieval is caused by pixels of a lower HDRF intensity located at the edge of spruce crowns. These AISA image pixels might be more affected by the background reflectance or they might contain a higher proportion of shadows than the one simulated by the RT models.

[Fig. 10 about here.]

The results of our retrieval methods are, in general, comparable with previously published airborne C_{ab} mapping efforts in coniferous canopies. For instance, Zarco-Tejada et al. (2004) up-scaled the simple ratio $SR_{750/710}$ using the PROSPECT and SPRINT RT models to map C_{ab} of sunlit Jack pine crowns, achieving an RMSE of 8.1 μg cm^{-2} (RRMSE of 27.0%, computed for a C_{ab} range between 26.8 and 56.8 μg cm^{-2}). Our $SR_{750/710}$ retrieval achieved an RMSE of 4.16 μg cm^{-2} (RRMSE of 7.97%). Moorthy et al. (2008) reported an RMSE of 5.3 μg cm^{-2} (RRMSE of 26.20% for a pigment range of 25.7 – 45.9 μg cm^{-2}), when estimating C_{ab} of pine needles using coupled leaf (LIBERTY and PROSPECT) and canopy (SAILH) RT models, and Zhang et al. (2008) estimated C_{ab} of Black spruce stands from CASI airborne data using PROSPECT and the 4-Scale geometrical–optical model with an accuracy of R^2 equal to 0.47 and an RMSE of 4.34 μg cm^{-2}. Our continuum removal based methods achieved the RMSE of almost two-folds lower than results of these studies. Finally, Schlerf et al. (2010) obtained an R^2 of 0.80 and RRMSE of 4.0% using a stepwise multiple linear regression predicting C_{ab} from continuum-removed Norway spruce reflectance functions of two HyMap airborne wavebands. Our ANN and $ANCB_{650-720}$ retrievals reached very similar RRMSE (Table 4b), with the systematic RMSE component always smaller than the unsystematic one. Still, it should be mentioned that none of the sampled crowns at our study site contained extremely low (≤ 15 μg cm^{-2}) or high (≥ 60 μg cm^{-2}) amounts of C_{ab}.

The cross-comparison of the C_{ab} values estimated for the nine ground-sampled crowns by $ANCB_{650-720}$ and ANN (Fig. 10c) indicates a similar result to the one in Fig. 9d. The figures show that although both approaches are based on continuum removal, the $ANCB_{650-720}$ estimates for low C_{ab} values are higher than those produced by the ANN. The ANN approach is, based on the validation results, slightly more accurate, but it is also more laborious and computationally intensive, especially during the training phase. Since ANN architecture contains several tuning parameters (e.g. the transitional functions between the neuron layers and their weights), it takes several hours and hundreds of training permutations to achieve the network of a desirable performance. The $ANCB_{650-720}$ approach is faster (it takes only few minutes to establish a relationship between the index and C_{ab} values), but still a comparably robust estimator, if applied to airborne images of high (sub-meter) spatial resolution that allows identification and exclusion of spectrally impure or noisy (e.g. deeply shadowed) canopy pixels.

4. Conclusions

This study demonstrates that leaf-canopy radiative transfer modeling combined with continuum removal of red and red-edge reflectance (650 – 720 nm) can be successfully used for the retrieval of coniferous C_{ab} using airborne imaging spectroscopy data at sub-meter spatial resolution. Results are suggesting that the C_{ab} estimation based on the continuum removal transformation of several adjacent spectral bands is more robust than the retrieval using optical indices computed from few discrete reflectance bands. The selected spectral range was shown to be sufficient to accurately retrieve C_{ab} of closed forest canopies with a LAI above four. Nonetheless, a more generalized applicability of the method might be achieved, when further tested for sensors with different technical specifications (e.g. spectral sampling interval and full-width-half-maximum).

The newly proposed C_{ab} index $ANCB_{650-720}$ outperformed three selected reflectance ratio based optical indices ($ND_{925\&710}$, $SR_{750/710}$ and TCARI/OSAVI) and performed comparably to an ANN trained to retrieve the leaf C_{ab} of spruce crowns using the continuum removed PROSPECT-DART simulations. The only weakness in $ANCB_{650-720}$ performance is a subtle overestimation of C_{ab} values below 30 $\mu g\ cm^{-2}$. With the systematic RMSE being lower than the unsystematic one, the newly proposed index is similarly robust, but faster, than ANN as no time-consuming training is required. Because of this, we recommend using $ANCB_{650-720}$ for retrieving C_{ab} when both high vegetation fraction and high signal-to noise ratio (as in case of sunlit canopy pixels) are present.

Properly validated high spatial resolution $ANCB_{650-720}$ C_{ab} maps could be used to validate satellite products at regional scale instead of conducting laborious, costly, and spatially limited field investigations. The remaining challenge is, however, to develop an operational gridding approach (Gómez-Chova et al., 2011) that would facilitate an accurate overlay of the airborne maps with satellite products of coarse spatial resolution.

Acknowledgement

This study was carried out within the ESA/PECS project No. 98029 (Global Change Research Centre, Academy of Sciences of the Czech Republic) using the CzeCOS infrastructure (LM2010007) supported by the CzechGlobe project (CZ.1.05/1.1.00/02.0073). Access to the MetaCentrum parallel computing clusters provided under the program 'Projects of Large Infrastructure for Research, Development, and Innovations' (LM2010005 funded by the Ministry of Education, Youth, and Sports of the Czech Republic) is acknowledged for facilitating our radiative transfer simulations. The work of authors from University of Zürich has been supported by the European Commission 6th Framework Programme project ECOCHANGE (GOCE-036866).

References

Bacour, C., Baret, F., Béal, D., Weiss, M., & Pavageau, K. (2006). Neural network estimation of *LAI*, *fAPAR*, *fCover* and $LAI{\times}C_{ab}$, from top of canopy MERIS reflectance data: Principles and validation. *Remote Sensing of Environment*, 105, 313-325.

Broge, N.H., & Leblanc, E. (2001). Comparing prediction power and stability of broadband and hyperspectral vegetation indices for estimation of green leaf area index and canopy chlorophyll density. *Remote Sensing of Environment*, 76, 156-172.

Buonasera, K., Lambreva, M., Rea, G., Touloupakis, E. & Giardi, M.T. (2009). Technological applications of chlorophyll a fluorescence for the assessment of environmental pollutants. *Analytical and Bioanalytical Chemistry*, 401, 1139-1151.

Clark, R.N., & Roush, T.L. (1984). Reflectance spectroscopy: Quantitative analysis techniques for remote sensing applications. *Journal of Geophysical Research*, 89, B7, 6329-6340.

Chen, M., Schliep, M., Willows, R.D., Cai, Z.-L., Neilan, B.A., & Scheer, H. (2010). A Red-Shifted Chlorophyll. *Science*, 329, 1318-1319.

Clevers, J.G.P.W. (1989). Application of a weighted infrared-red vegetation index for estimating Leaf Area Index by Correcting for Soil Moisture. *Remote Sensing of Environment*, 29, 25-37.

Combal, B., Baret, F., Weiss, M., Trubuil, A., Macé, D., Pragnère, A., Myneni, R., Knyazikhin, Y., & Wang, L. (2003). Retrieval of canopy biophysical variables from bidirectional reflectance: Using prior information to solve the ill-posed inverse problem. *Remote Sensing of Environment*, 84, 1-15.

Curran, P.J. (1989). Remote sensing of foliar chemistry. *Remote Sensing of Environment*, 30, 271-278.

Curran, P.J., Dungan, J.L., & Peterson, D.L. (2001). Estimating the foliar biochemical concentration of leaves with reflectance spectrometry: Testing the Kokaly and Clark methodologies. *Remote Sensing of Environment*, 76, 349-359.

Dash, J., Jeganathan, C., & Atkinson, P.M. (2010). The use of MERIS Terrestrial Chlorophyll Index to study spatio-temporal variation in vegetation phenology over India. *Remote Sensing of Environment*, 114, 1388-1402.

Daughtry, C.S.T., Walthall, C.L., Kim, M.S., Brown de Colstoun, E., & McMurtrey III, J.E. (2000). Estimating corn leaf chlorophyll concentration from leaf and canopy reflectance. *Remote Sensing of Environment*, 74, 229-239.

Disney, M., Lewis, P., & North, P.R.J. (2000). Monte Carlo ray tracing in optical canopy reflectance modeling. *Remote Sensing Reviews*, 18, 163-196.

Disney, M., Lewis, P., & Saich, P. (2006). 3D modelling of forest canopy structure for remote sensing simulations in the optical and microwave domains. *Remote Sensing of Environment*, 100, 114-132.

Feret, J.B., Francois, C., Asner, G.P., Gitelson, A.A., Martin, R.E., Bidel, L.P.R., Ustin, S.L., le Maire, G., & Jacquemoud, S. (2008). PROSPECT-4 and 5: Advances in the leaf optical properties model separating photosynthetic pigments. *Remote Sensing of Environment*, 112, 3030-3043.

Gastellu-Etchegorry, J.P., Demarez, V., Pinel, V., & Zagolski, F. (1996). Modeling radiative transfer in heterogeneous 3-D vegetation canopies. *Remote Sensing of Environment*, 58, 131-156.

Gastellu-Etchegorry, J.P., Martin, E., & Gascon, F. (2004). DART: a 3D model for simulating satellite images and studying surface radiation budget. *International Journal of Remote Sensing*, 25, 73-96.

Gitelson, A.A., Gritz, Y., & Merzlyak, M.N. (2003). Relationships between leaf chlorophyll content and spectral reflectance and algorithms for non-destructive chlorophyll assessment in higher plant leaves. *Journal of plant physiology*, 160, 271-282.

Gitelson, A.A., Keydan, G.P., & Merzlyak, M.N. (2006). Three-band model for noninvasive estimation of chlorophyll, carotenoids, and anthocyanin contents in higher plant leaves. *Geophysical Research Letters*, 33, 1-5.

Gitelson, A.A., Merzlyak, M.N., & Lichtenthaler, H.K. (1996). Detection of Red Edge Position and Chlorophyll Content by Reflectance Measurements Near 700 nm. *Journal of Plant Physiology*, 148, 501-508.

Gómez-Chova, L., Zurita-Milla, R., Alonso, L., Amorós-López, J., Guanter, L., & Camps-Valls, G. (2011). Gridding Artifacts on Medium-Resolution Satellite Image Time

Series: MERIS Case Study. *IEEE Transactions on Geosciences and Remote Sensing*, 49, 2601-2611.

Haboudane, D., Miller, J.R., Tremblay, N., Zarco-Tejada, P.J., & Dextraze, L. (2002). Integrated narrow-band vegetation indices for prediction of crop chlorophyll content for application to precision agriculture. *Remote Sensing of Environment*, 81, 416-426.

Harris, A., & Dash, J. (2010). The potential of the MERIS Terrestrial Chlorophyll Index for carbon flux estimation. *Remote Sensing of Environment*, 114, 1856-1862.

Homolová, L., Lukeš, P., Malenovský, Z., Lhotáková, Z., Kaplan, V., Hanuš, J. (2012). Measurement and variability assessment of the Norway spruce total leaf area: Implications for remote sensing. *Trees – Structure and Function*, in print.

Jacquemoud, S., & Baret, F. (1990). PROSPECT: A model of leaf optical properties spectra. *Remote Sensing of Environment*, 34, 75-91.

Jacquemoud, S., Ustin, S.L., Verdebout, J., Schmuck, G., Andreoli, G., & Hosgood, B. (1996). Estimating leaf biochemistry using the PROSPECT leaf optical properties model. *Remote Sensing of Environment*, 56, 194-202.

Jordan, C.F. (1969). Derivation of leaf area index from quality of light on the forest floor. *Ecology*, 50, 663–666.

Kimes, D.S., & Kirchner, J.A. (1982). Radiative transfer model for heterogeneous 3d scenes. *Applied Optics*, 21, 4119-4129.

Knox, N.M., Skidmore, A.K., Prins, H.H.T., Asner, G.P., van der Werff, H.M.A., de Boer, W.F., van der Waal, C., de Knegt, H.J., Kohi, E.M., Slotow, R., & Grant, R.C. (2011). Dry season mapping of savanna forage quality, using the hyperspectral Carnegie Airborne Observatory sensor. *Remote Sensing of Environment*, 115, 1478-1488.

Kokaly, R.F., & Clark, R.N. (1999). Spectroscopic determination of leaf biochemistry using band-depth analysis of absorption features and stepwise multiple linear regression. *Remote Sensing of Environment*, 67, 267-287.

Kokaly, R.F., Despain, D.G., Clark, R.N., & Livo, K.E. (2003). Mapping vegetation in Yellowstone National Park using spectral feature analysis of AVIRIS data. *Remote Sensing of Environment*, 84, 437-456.

le Maire, G., Francois, C., Soudani, K., Berveiller, D., Pontailler, J.-Y., Breda, N., Genet, H., Davi, H., & Dufrene, E. (2008). Calibration and validation of hyperspectral indices for the estimation of broadleaved forest leaf chlorophyll content, leaf mass per area, leaf area index and leaf canopy biomass. *Remote Sensing of Environment*, 112, 3846-3864.

Liu, J., Miller, J.R., Haboudane D., & Pattey, E. (21-25 September, 2004). Exploring the Relationship Between Red Edge Parameters and Crop Biophysical Variables for Precision Agriculture, *Proceedings IEEE International Geoscience and Remote Sensing Symposium (IGARSS '04*) (pp 1276-1279), Fairbanks, Alaska, USA.

Lhotáková, Z., Albrechtová ,J., Malenovský, Z., Rock, B.N., Polák, T., & Cudlín, P. (2007). Does the azimuth orientation of Norway spruce (Picea abies /L./ Karst.) branches within sunlit crown part influence the heterogeneity of biochemical, structural and spectral characteristics of needles? *Environmental and Experimental Botany*, 59, 283-292.

Malenovský, Z., Albrechtová, J.,Lhotáková, Z., Zurita-Milla, R., Clevers, J.G.P.W., Schaepman, M.E., & Cudlín, P. (2006). Applicability of the PROSPECT model for Norway spruce needles. *International Journal of Remote Sensing*, 27, 5315-5340.

Malenovský, Z., Martin, E., Homolová, L., Gastellu-Etchegorry, J. P., Zurita-Milla, R., Schaepman, M.E., Pokorný, R., Clevers, J.G.P.W., & Cudlín, P. (2008). Influence of woody elements of a Norway spruce canopy on nadir reflectance simulated by the

DART model at very high spatial resolution. *Remote Sensing of Environment*, 112, 1-18.

Moorthy, I., Miller, J.R., & Noland, T.L. (2008). Estimating chlorophyll concentration in conifer needles with hyperspectral data: an assessment at the needle and canopy level. *Remote Sensing of Environment*, 112, 2824-2838.

Myneni, R.B. (1991). Modeling radiative transfer and photosynthesis in three-dimensional vegetation canopies. *Agricultural and Forest Meteorology*, 55, 323-344.

Myneni, R.B., Asrar, G., & Hall, F.G. (1992). A three-dimensional radiative transfer method for optical remote sensing of vegetated land surfaces. *Remote Sensing of Environment*, 41, 105-121.

Normile, D. (2009). Round and Round: A Guide to the Carbon Cycle. *Science*, 325, 1642-1643.

Písek, J., Chen, J.M., & Nilson, T. (2011). Estimation of vegetation clumping index using MODIS BRDF data. *International Journal of Remote Sensing*, 32, 2645-2657.

Pokorný, R., & Marek, M.V. (2000). Test of accuracy of LAI estimation by LAI-2000 under artificially changed leaf to wood area proportions. *Biologia Plantarum*, 43, 537-544.

Porra, R.J., Thompson, W.A., & Kriedemann, P.E. (1989). Determination of accurate extinction coefficients and simultaneous equations for assaying chlorophylls a and b extracted with four different solvents: verification of the concentration of chlorophyll standards by atomic absorption spectroscopy. *Biochemica and Biophysica Acta,* 975, 384-394.

Richter, R., & Schläpfer, D. (2002). Geo-atmospheric processing of airborne imaging spectrometry data. Part 2: atmospheric/topographic correction. *International Journal of Remote Sensing*, 23, 2631-2649.

Schaepman, M.E., Ustin, S.L., Plaza, A.J., Painter, T.H., Verrelst, J., & Liang, S. (2009). Earth system science related imaging spectroscopy - An assessment. *Remote Sensing of Environment*, 113, S123-S137.

Schaepman-Strub, G., Schaepman, M.E., Painter, T.H., Dangel, S., & Martonchik, J.V. (2006). Reflectance quantities in optical remote sensing — definitions and case studies. *Remote Sensing of Environment*, 103, 27-42.

Schlerf, M., Atzberger, C., Hill, J., Buddenbaum, H., Werner, W., & Schüler, G. (2010). Retrieval of chlorophyll and nitrogen in Norway spruce (Picea abies L. Karst.) using imaging spectroscopy. *International Journal of Applied Earth Observation and Geoinformation*, 12, 17–26.

Schmidt, K.S., & Skidmore, A.K. (2003). Spectral discrimination of vegetation types in a coastal wetland. *Remote Sensing of Environment*, 85, 92-108.

Smith, G.M., & Milton, E.J. (1999). The use of the empirical line method to calibrate remotely sensed data to reflectance. *International Journal of Remote Sensing*, 20, 2653-2662.

Smolander, S., & Stenberg, P. (2003). A method to account for shoot scale clumping in coniferous canopy reflectance models. *Remote Sensing of Environment*, 88, 363-373.

Stagakis, S., Markos, N., Sykioti, O., & Kyparissis, A. (2010). Monitoring canopy biophysical and biochemical parameters in ecosystem scale using satellite hyperspectral imagery: An application on a *Phlomis fruticosa* Mediterranean ecosystem using multiangular CHRIS/PROBA observations. *Remote Sensing of Environment*, 114, 977-994.

Stenberg, P. (1996). Simulations of the effects of shoot structure and orientation on vertical gradients in intercepted light by conifer canopies. *Tree Physiology*, 16, 99-108.

Tucker, C.J. (1979). Red and photographic infrared linear combinations for monitoring vegetation. *Remote Sensing of Environment*, 8, 127−150.

Underwood, E., Ustin, S.L., & DiPietro, D. (2003). Mapping nonnative plants using hyperspectral imagery. *Remote Sensing of Environment*, 86, 150-161.

Urban, O., Janouš, D., Acosta, M., Czerný, R., Marková, I., Navrátil, M., Pavelka, M., Pokorný, R., Šprtová, M., Zhang, R., Špunda, V., Grace, J., & Marek, M.V. (2007). Ecophysiological controls over the net ecosystem exchange of mountain spruce stand. Comparison of the response in direct vs. diffuse solar radiation. G*lobal Change Biology*, 13, 157–168.

Ustin, S.L., Gitelson, A.A. , Jacquemoud, S., Schaepman, M., Asner, G.P., Gamon, J.A., & Zarco-Tejada, P. (2009). Retrieval of foliar information about plant pigment systems from high resolution spectroscopy. *Remote Sensing of Environment*, 113, S67-S77.

Verrelst, J., Schaepman, M.E., Malenovský, Z., & Clevers J.G.P.W. (2010). Effects of woody elements on simulated canopy reflectance: Implications for forest chlorophyll content retrieval. *Remote Sensing of Environment*, 114, 647-656.

Wellburn, A.R. (1994). The spectral determination of chlorophyll a and chlorophhyll b, as well as total carotenoids, using various solvents with spectrophotometers of different resolution. *Journal of Plant Physiology*, 144, 307-313.

Widlowski, J.-L.. Pinty, B., Lavergne, T., Verstraete, M.M., & Gobron N. (2006). Horizontal radiation transport in 3-D forest canopies at multiple spatial resolutions: Simulated impact on canopy absorption. *Remote Sensing of Environment*, 103, 379-397.

Widlowski, J.-L., Robustelli, M., Disney, M., Gastellu-Etchegorry, J.-P., Lavergne, T., Lewis, P., North, P.R.J., Pinty, B., Thompson, R., & Verstraete, M.M. (2008). The RAMI On-line Model Checker (ROMC): A web-based benchmarking facility for canopy reflectance models. *Remote Sensing of Environment*, 112, 1144−1150.

Willmott, C.J. (1981). On the validation of models. *Physical Geography*, 2, 184-194.

Youngentob, K.N., Roberts, D.A, Held, A.A, Dennison, P.E., Jia, X., & Lindenmayer, D.B. (2011). Mapping two Eucalyptus subgenera using multiple endmember spectral mixture analysis and continuum-removed imaging spectrometry data. *Remote Sensing of Environment*, 115, 1115-1128.

Zarco-Tejada, P.J., Miller, J.R., Harron, J., Hu, B., Noland, T.L., Goel, N., Mohammed, G.H., & Sampson, P. (2004). Needle chlorophyll content estimation through model inversion using hyperspectral data from boreal conifer forest canopies. *Remote Sensing of Environment*, 89, 189–199.

Zarco-Tejada, P.J., Miller, J.R., Noland, T.L., Mohammed, G.H., & Sampson, P.H. (2001). Scaling-up and model inversion methods with narrowband optical indices for chlorophyll content estimation in closed forest canopies with hyperspectral data. *IEEE Transactions on Geoscience and Remote Sensing*, 39, 1491-1507.

Zhang, Y., Chen, J.M., Miller, J.R., & Noland, T.L. (2008). Leaf chlorophyll content retrieval from airborne hyperspectral remote sensing imagery. *Remote Sensing of Environment*, 112, 3234-3247.

List of Tables

Table 1.

Fixed and varied key input parameters for DART radiative transfer simulations of a Norway spruce scene.

p. 10

Table 2.

Fixed input parameters for PROSPECT radiative transfer simulations of Norway spruce needle optical properties (C_w ~ leaf water column, C_m ~ leaf mass per area, N ~ leaf mesophyll structural parameter, C ~ needles of the current growing season, C+1 ~ needles of the previous growing season, and C++ ~ needles older than the previous growing season).

p. 11

Table 3.

Relative weights for sun-exposed and shaded crown parts per needle age-class used to compute the single mean leaf chlorophyll *a* & *b* content of sampled Norway spruce crown. (C ~ needles of the current growing season, C+1 ~ needles of the previous growing season, and C++ ~ needles older than the previous growing season).

p. 16

Table 4.

Results of statistical analyses comparing the leaf chlorophyll *a* & *b* content (C_{ab}) estimated for sunlit spruce crown pixels of the AISA Eagle airborne image with four optical indices ($ANCB_{650-720}$, $ND_{925\&710}$, $SR_{750/710}$ and ratio TCARI/OSAVI) and with an artificial neural network (ANN) approach (a), and assessing their prediction accuracy when compared with ground measured crown C_{ab} values (b). (R^2 ~ coefficient of determination of the linear function, RMSE ~ root mean square error, RRMSE ~ relative RMSE computed for the actual chlorophyll range of 14.7 – 66.9 μg cm^{-2}, $RMSE_s$ ~ systematic RMSE, $RMSE_u$ ~ unsystematic RMSE, and *d* ~ index of agreement).

p. 24

List of Figures

Fig. 1.

Basic methodological steps of the study. Rectangular objects represent the input/output data or models, while ellipsoidal objects represent the data processing and other operations (C_{ab} ~ leaf chlorophyll *a* & *b* content, ANN ~ Artificial Neural Network, AISA ~ Airborne Imaging Spectroradiometer).

p. 6

Fig. 2.

AISA Eagle image subset of Norway spruce forest stand at the research site Bílý Kříž (a) (yellow polygons indicate the locations of ten sunlit tree crowns selected for ground truth sampling) and the maximum likelihood automatic classification separating sunlit and shaded spruce crowns from the background (b).

p. 8

Fig. 3.

The mean top-of-the-canopy reflectance factor of 60 AISA Eagle spectral bands for all pixels classified as sunlit and shaded spruce crowns (n = 151984 and 137305, respectively). The solid line with full circular symbols represents the mean AISA reflectance of nine sunlit crowns used in validation of the airborne remote sensing C_{ab} estimates. Dashed lines represent the reflectance +/- standard deviations.

p. 8

Fig. 4.

Selection of the spectral interval for continuum removal of chlorophyll sensitive wavelengths: start of the continuum at 650 nm (in the middle of the chlorophyll *a* & *b* (C_{ab}) specific absorption feature from 550 to 750 nm) and end of the continuum at 720 nm (in the middle of the red edge reflectance from 680 to 760 nm).

p. 9

Fig. 5.

Sensitivity of continuum removed reflectance between 650 and 720 nm to leaf chlorophyll content (C_{ab}) and leaf area index for six spectral bands simulated by the PROSPECT-DART radiative transfer models at: 661.41 (a), 670.74 (b), 680.06 (c), 689.39 (d), 698.72 (e), and 708.07 nm (f). Each line corresponds with a simulated C_{ab} level (C_{ab} ~ 10, 25, 40, 55, 70, and 80 μg cm^{-2}). Small error bars represent positive and negative standard deviations driven by simulated canopy closures (CC ~ 75, 85, and 95%).

p. 19

Fig. 6.

Design of the $ANCB_{650\text{-}720}$ optical index (c) using the Area Under Curve ($AUC_{650\text{-}720}$) of continuum removed reflectance (a) normalized by the Continuum Band Depth at 670 nm (CBD_{670}) (b), the relation between leaf chlorophyll content (C_{ab}) and Normalized Difference between reflectance at 925 and 710 nm ($ND_{925\&710}$) (d), Simple reflectance Ratio between 750 and 710 nm ($SR_{750/710}$) (e) and ratio TCARI/OSAVI (f). The equations represent the best fitting functions with the highest coefficient of determination (R^2). A single diamond symbol represents one of the PROSPECT-DART simulated leaf area index (LAI) values (LAI ~ <4, 9> with a step of 1) within three predefined canopy closures (CC ~ 75, 85 and 95%).

p. 20

Fig. 7.

Leaf chlorophyll content of sunlit Norway spruce crown pixels estimated by ANN (a), $ANCB_{650\text{-}720}$ (b), and their reciprocal difference ($ANCB_{650\text{-}720}$ – ANN) (c), including histograms showing the percentage of pixels per C_{ab} class estimated by ANN (d), by $ANCB_{650\text{-}720}$ (e), and the distribution of C_{ab} differences between both methods (f).

p. 23

Fig. 8.

Histograms showing the percentage of sunlit crown pixels per C_{ab} value estimated by the Normalized Difference between reflectance at 925 and 710 nm ($ND_{925\&710}$) (a), Simple reflectance Ratio between 750 and 710 nm ($SR_{750/710}$) (b) and ratio TCARI/OSAVI (c), and the distribution of estimated C_{ab} differences computed between all three optical indices and the ANN (d, e, f).

p. 23

Fig. 9.

Scatterplot of leaf chlorophyll content (C_{ab}) retrieved by artificial neural network (ANN) plotted against the C_{ab} estimates of Normalized Difference ($ND_{925\&710}$) (a), Simple reflectance Ratio ($SR_{750/710}$) (b), ratio of TCARI/OSAVI indices (c) and $ANCB_{650\text{-}720}$ optical index (d). Each dot symbol represents one pixel of a sunlit tree crown identified in the AISA Eagle image of the test site (R^2 ~ coefficient of determination, RMSE ~ root mean square error).

p. 24

Fig. 10.

Validation of leaf chlorophyll content (C_{ab}) retrieved for the sampled spruce crowns from the AISA Eagle image using artificial neural network (ANN) (a), $ANCB_{650\text{-}720}$ optical index (b), Normalized Difference between reflectance at 925 and 710 nm ($ND_{925\&710}$) (d), Simple reflectance Ratio between 750 and 710 nm ($SR_{750/710}$) (e), ratio TCARI/OSAVI (f) and the reciprocal comparison of ANN and $ANCB_{650-720}$ estimations (c). Each circle represents one tree crown, horizontal bars represent two standard deviations of C_{ab} values either measured on the ground or retrieved by ANN and optical indices. (R^2 ~ coefficient of determination, RMSE ~ root mean square error).

p. 25

Tables

Table 1.

Fixed and varied key input parameters for DART radiative transfer simulations of a Norway spruce scene.

Sun position (fixed)			/Real solar noon/
Zenith angle	θ_s	[°]	47.8
Azimuth angle (from North clockwise)	ϕ_s	[°]	183.4
Scene parameters	/representing a 25 year old Norway spruce forest stand/		
Voxel size (fixed)		[m]	0.2
Horizontal dimensions (fixed)	x, y	[m]	6.0, 6.0
Slope (fixed)		[°]	13.5
Number of tree crowns (varied)			4-7
Canopy closure (varied)	CC	[%]	75-95 /in steps of 10/
Leaf area index (varied)	LAI	[m^2 m^{-2}]	4.0-9.0 /in steps of 1.0/
Simulated AISA Eagle spectral bands	/Full-width-half-maximum – FWHM = 10 nm/		
Central wavelengths of visible (VIS) bands (fixed)	λ_{VIS}	[nm]	652.1, 661.4, 670.7, 680.1, 689.4
Central wavelengths of near infrared (NIR) bands (fixed)	λ_{NIR}	[nm]	698.7, 708.1, 717.4

Table 2.

Fixed input parameters for PROSPECT radiative transfer simulations of Norway spruce needle optical properties (C_w ~ leaf water column, C_m ~ leaf mass per area, N ~ leaf mesophyll structural parameter, C ~ needles of the current growing season, C+1 ~ needles of the previous growing season, and C++ ~ needles older than the previous growing season).

PROSPECT parameters / *Needle types*	C_w [cm]	C_m [g cm^{-2}]	N
Sunlit C	0.0475	0.0177	2.08
Sunlit C+1	0.0486	0.0206	2.08
Sunlit C++	0.0365	0.0233	2.08
Shaded C	0.0479	0.0118	2.02
Shaded C+1	0.0430	0.0172	2.02
Shaded C++	0.0461	0.0170	2.02

Table 3.

Relative weights for sun-exposed and shaded crown parts per needle age-class used to compute the single mean leaf chlorophyll *a* & *b* content of sampled Norway spruce crown. (C ~ needles of the current growing season, C+1 ~ needles of the previous growing season, and C++ ~ needles older than the previous growing season).

Branch Age-class	Sun-exposed [rel.]	Shaded [rel.]
C	0.230	0.057
C+1	0.224	0.089
C++	0.095	0.306

Table 4.

Results of statistical analyses comparing the leaf chlorophyll *a* & *b* content (C_{ab}) estimated for sunlit spruce crown pixels of the AISA Eagle airborne image with four optical indices ($ANCB_{650-720}$, $ND_{925\&710}$, $SR_{750/710}$ and ratio TCARI/OSAVI) and with an artificial neural network (ANN) approach (a), and assessing their prediction accuracy when compared with ground measured crown C_{ab} values (b). (R^2 ~ coefficient of determination of the linear function, RMSE ~ root mean square error, RRMSE ~ relative RMSE computed for the actual chlorophyll range of 14.7 – 66.9 μg cm^{-2}, $RMSE_s$ ~ systematic RMSE, $RMSE_u$ ~ unsystematic RMSE, and *d* ~ index of agreement).

(a) *ANN AISA estimates vs.*	R^2 [rel.]	RMSE [μg cm^{-2}]	RRMSE [%]	$RMSE_s$ [μg cm^{-2}]	$RMSE_u$ [μg cm^{-2}]	*d* [rel.]
$ANCB_{650-720}$	0.85	2.42	4.64	1.59	1.82	0.95
$ND_{925\&710}$	0.51	10.42	19.96	9.03	5.20	0.60
$SR_{750/710}$	0.52	6.10	11.69	4.63	3.98	0.75
TCARI/OSAVI	0.35	14.93	28.60	13.32	6.74	0.45
(b) *Ground measurements vs.*						
ANN	0.72	2.18	4.18	0.77	2.04	0.92
$ANCB_{650-720}$	0.72	2.27	4.35	1.59	1.62	0.89
$ND_{925\&710}$	0.64	9.07	17.38	8.75	2.40	0.53
$SR_{750/710}$	0.71	4.16	7.97	3.82	1.64	0.75
TCARI/OSAVI	0.41	12.30	23.56	11.76	3.61	0.42

Figures

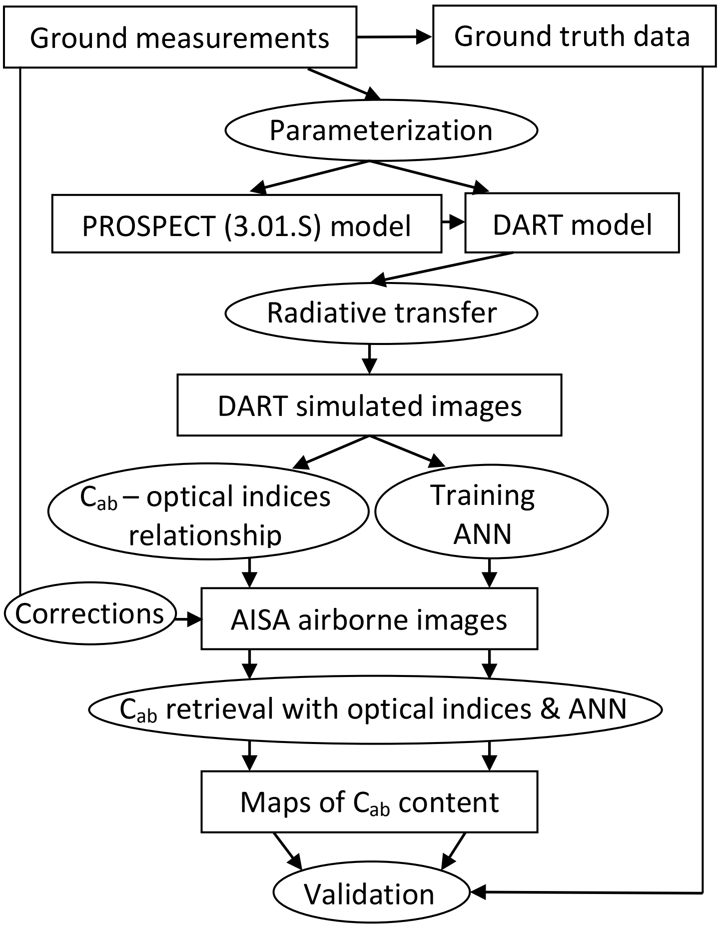

Fig. 1. Basic methodological steps of the study. Rectangular objects represent the input/output data or models, while ellipsoidal objects represent the data processing and other operations (C_{ab} ~ leaf chlorophyll *a* & *b* content, ANN ~ Artificial Neural Network, AISA ~ Airborne Imaging Spectroradiometer).

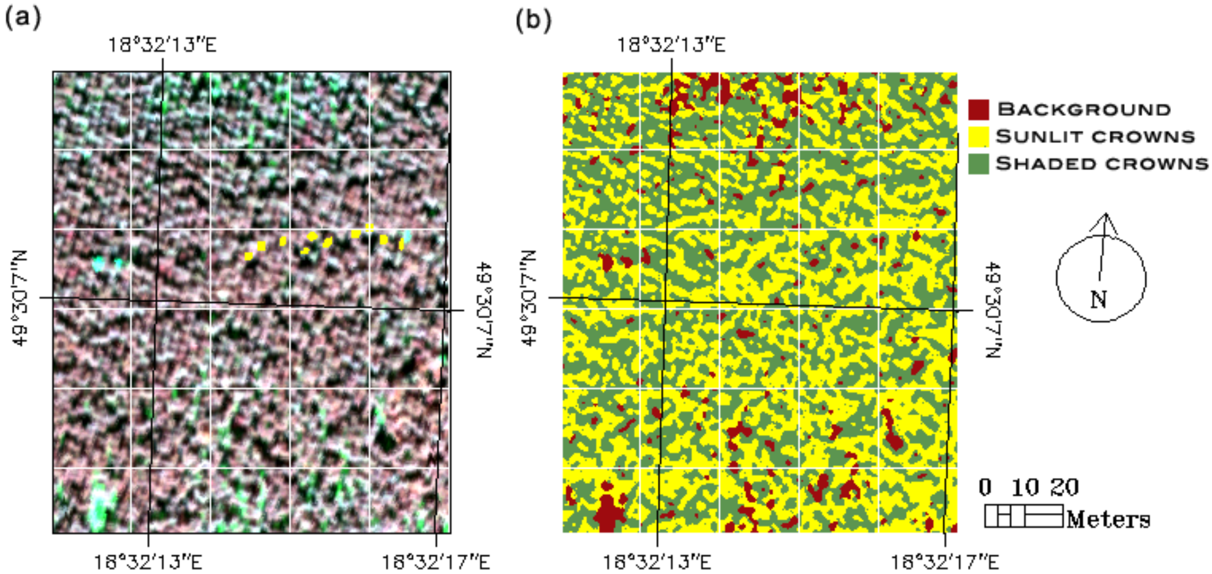

Fig. 2. AISA Eagle image subset of Norway spruce forest stand at the research site Bílý Kříž (a) (yellow polygons indicate the locations of ten sunlit tree crowns selected for ground truth sampling) and the maximum likelihood automatic classification separating sunlit and shaded spruce crowns from the background (b).

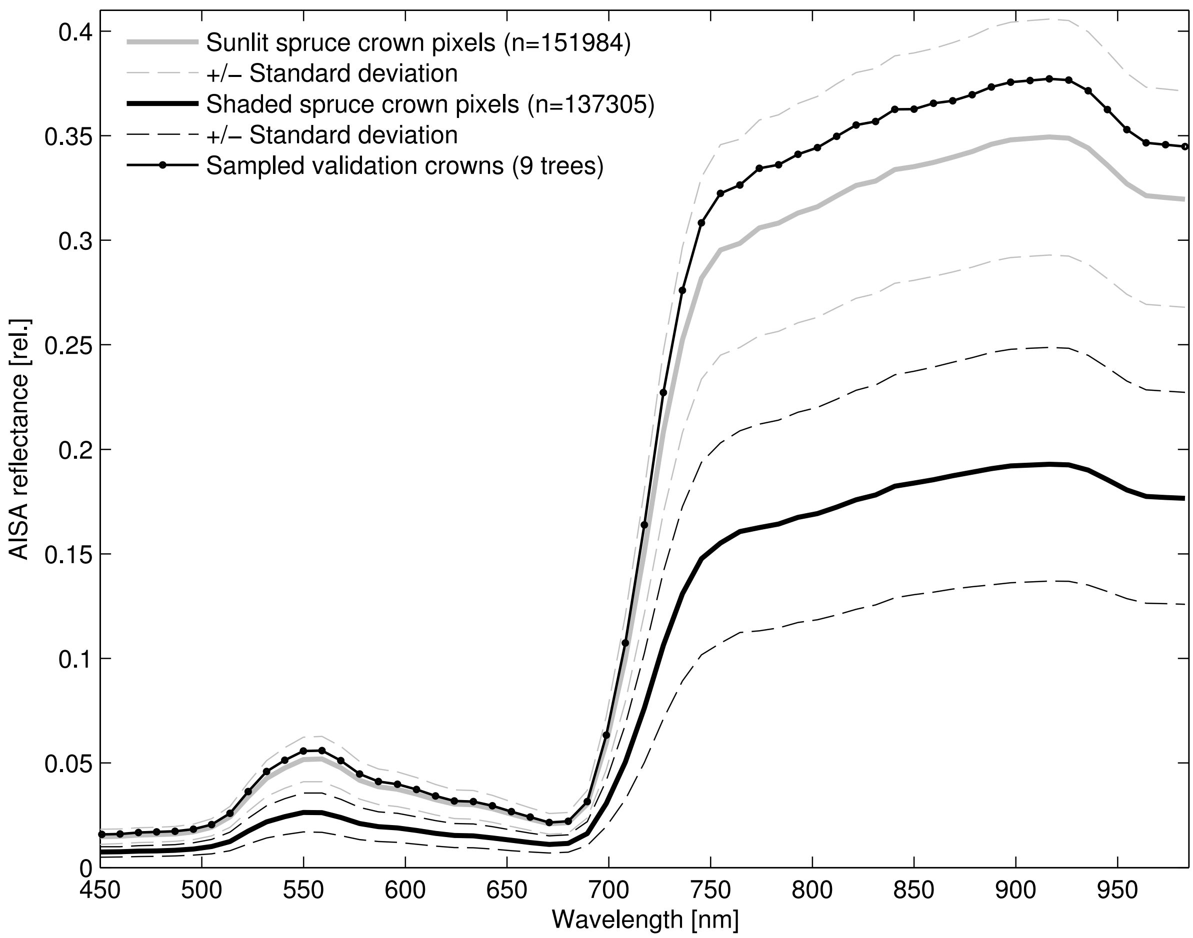

Fig. 3. The mean top-of-the-canopy reflectance factor of 60 AISA Eagle spectral bands for all pixels classified as sunlit and shaded spruce crowns (n = 151984 and 137305, respectively). The solid line with full circular symbols represents the mean AISA reflectance of nine sunlit crowns used in validation of the airborne remote sensing C_{ab} estimates. Dashed lines represent the reflectance +/- standard deviations.

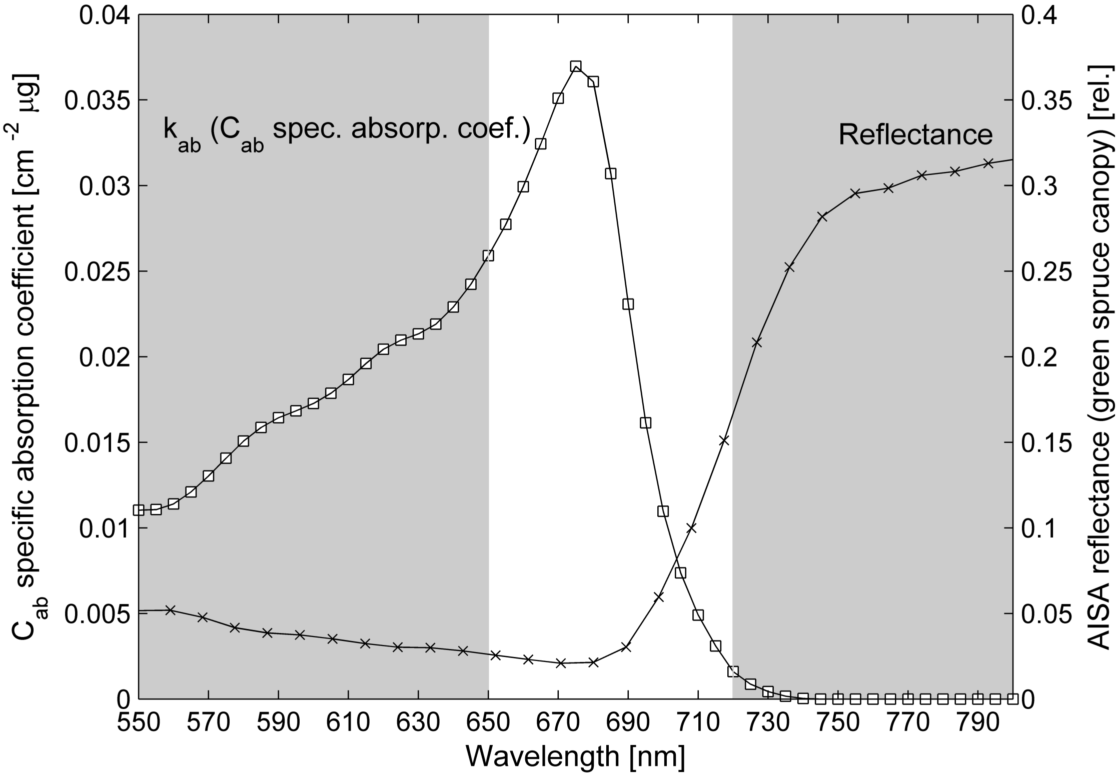

Fig. 4. Selection of the spectral interval for continuum removal of chlorophyll sensitive wavelengths: start of the continuum at 650 nm (in the middle of the chlorophyll *a* & *b* (C_{ab}) specific absorption feature from 550 to 750 nm) and end of the continuum at 720 nm (in the middle of the red edge reflectance from 680 to 760 nm).

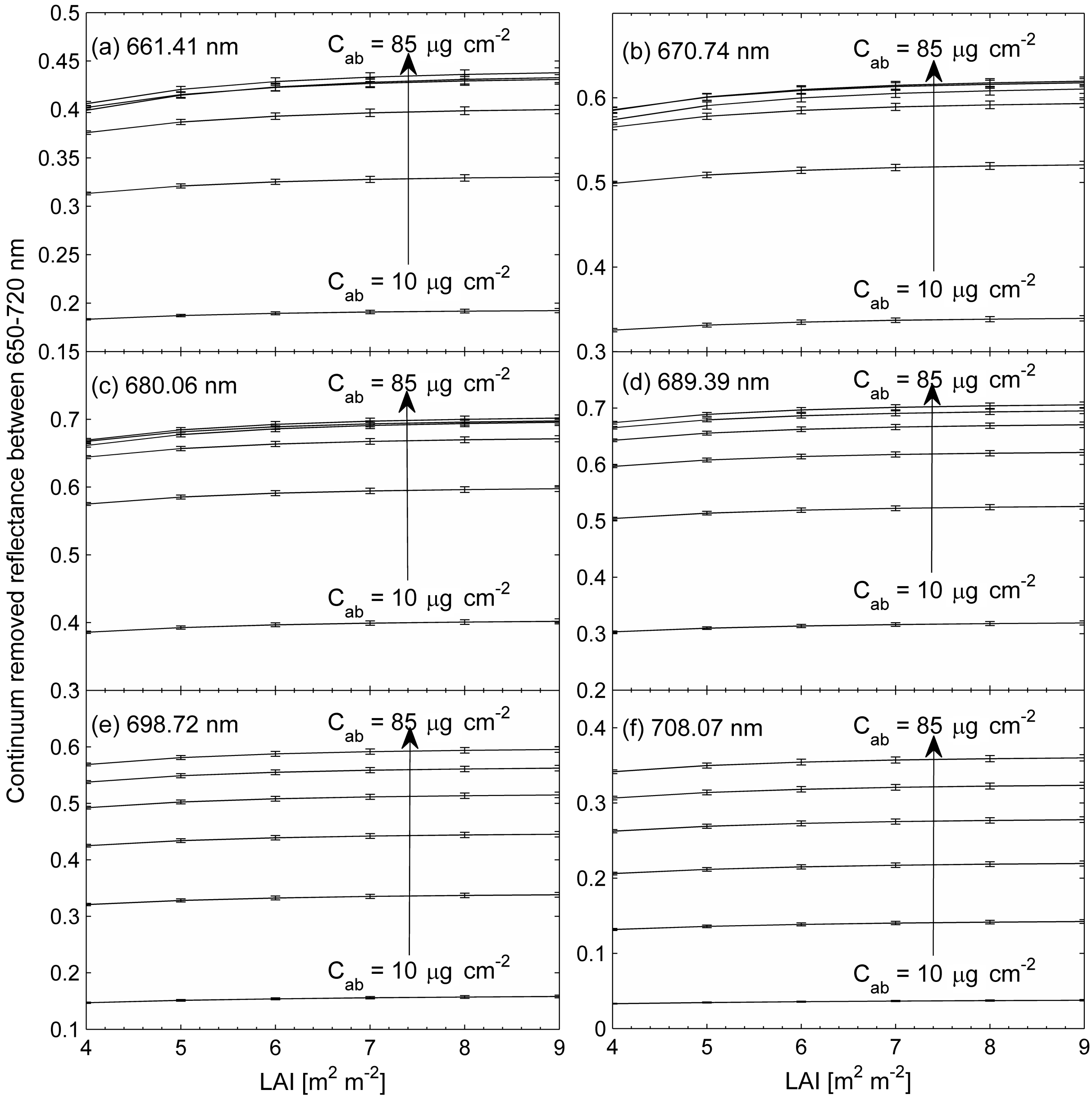

Fig. 5. Sensitivity of continuum removed reflectance between 650 and 720 nm to leaf chlorophyll content (C_{ab}) and leaf area index for six spectral bands simulated by the PROSPECT-DART radiative transfer models at: 661.41 (a), 670.74 (b), 680.06 (c), 689.39 (d), 698.72 (e), and 708.07 nm (f). Each line corresponds with a simulated C_{ab} level (C_{ab} ~ 10, 25, 40, 55, 70 and 85 μg cm^{-2}). Small error bars represent positive and negative standard deviations driven by simulated canopy closures (CC ~ 75, 85 and 95%).

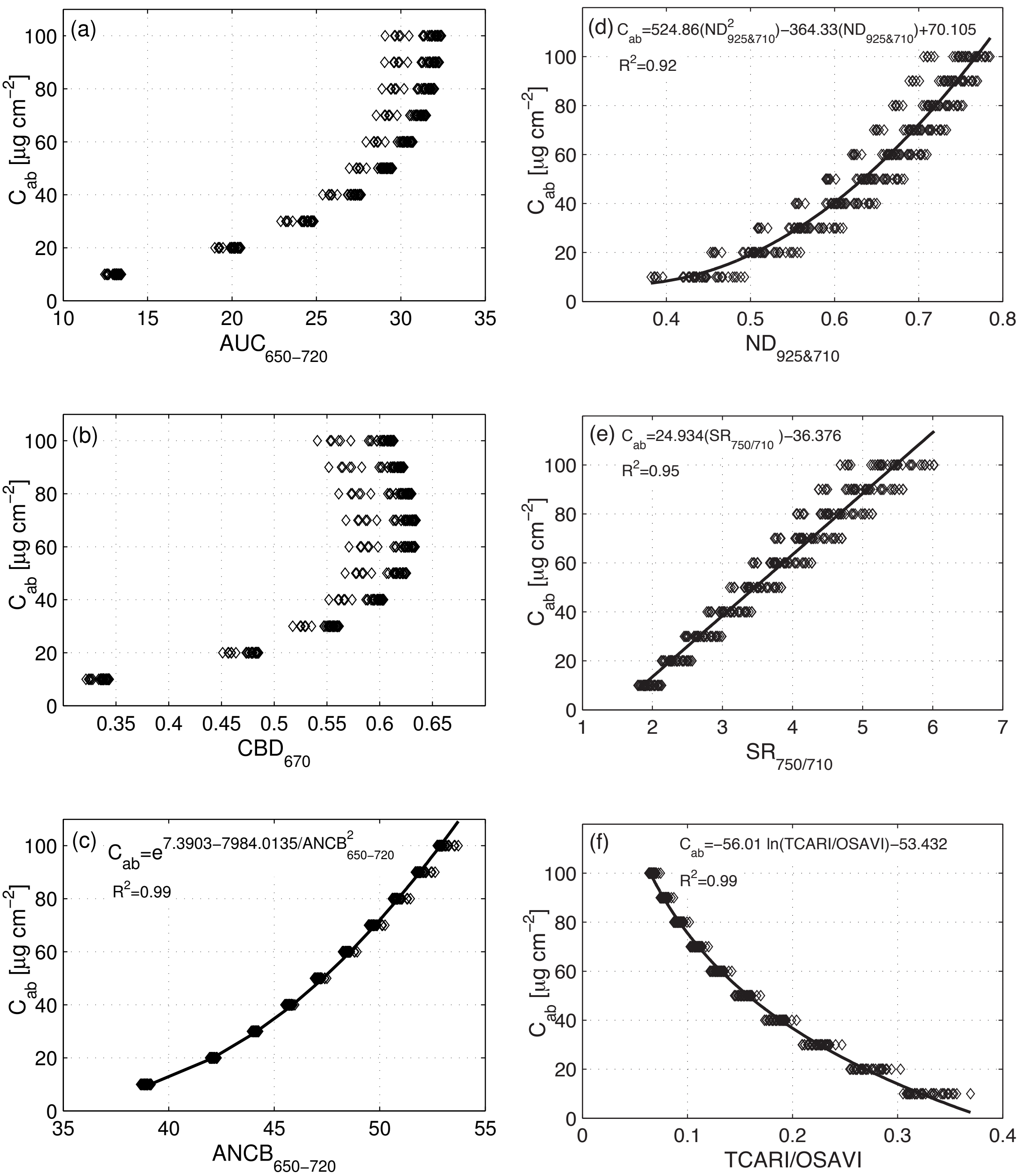

Fig. 6. Design of the $ANCB_{650-720}$ optical index (c) using the Area Under Curve ($AUC_{650-720}$) of continuum removed reflectance (a) normalized by the Continuum Band Depth at 670 nm (CBD_{670}) (b); relation between leaf chlorophyll content (C_{ab}) and Normalized Difference between reflectance at 925 and 710 nm ($ND_{925\&710}$) (d), Simple reflectance Ratio between 750 and 710 nm ($SR_{750/710}$) (e) and ratio TCARI/OSAVI (f). The equations represent the best fitting functions with the highest coefficient of determination (R^2). A single diamond symbol represents one of the PROSPECT-DART simulated leaf area index (LAI) values (LAI ~ <4, 9> with a step of 1) within three predefined canopy closures (CC ~ 75, 85 and 95%).

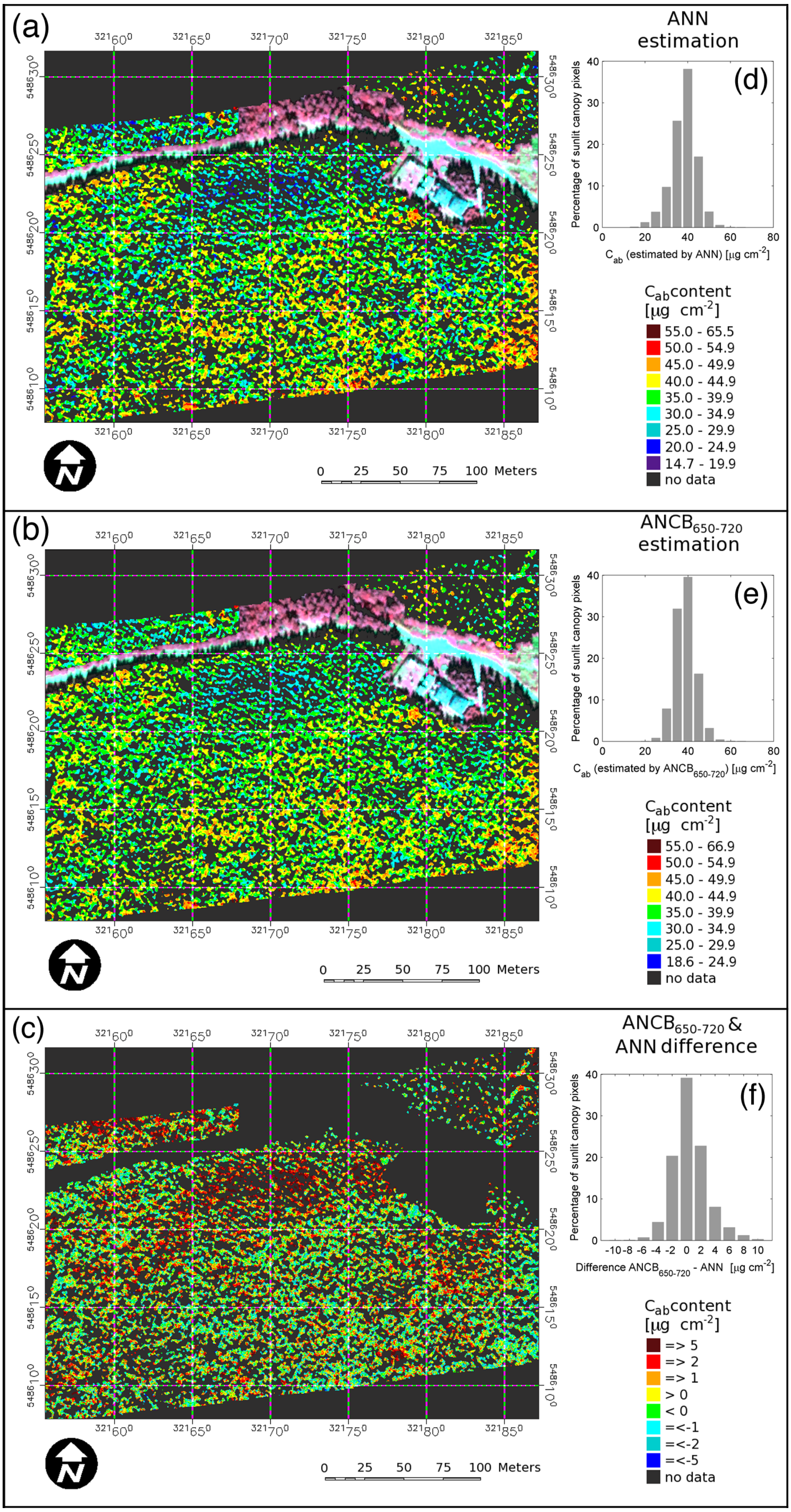

Fig. 7. Leaf chlorophyll content of sunlit Norway spruce crown pixels estimated by ANN (a), $ANCB_{650-720}$ (b), and their reciprocal difference ($ANCB_{650-720}$ – ANN) (c), including histograms showing the percentage of pixels per C_{ab} class estimated by ANN (d), by $ANCB_{650-720}$ (e), and the distribution of C_{ab} differences between both methods (f).

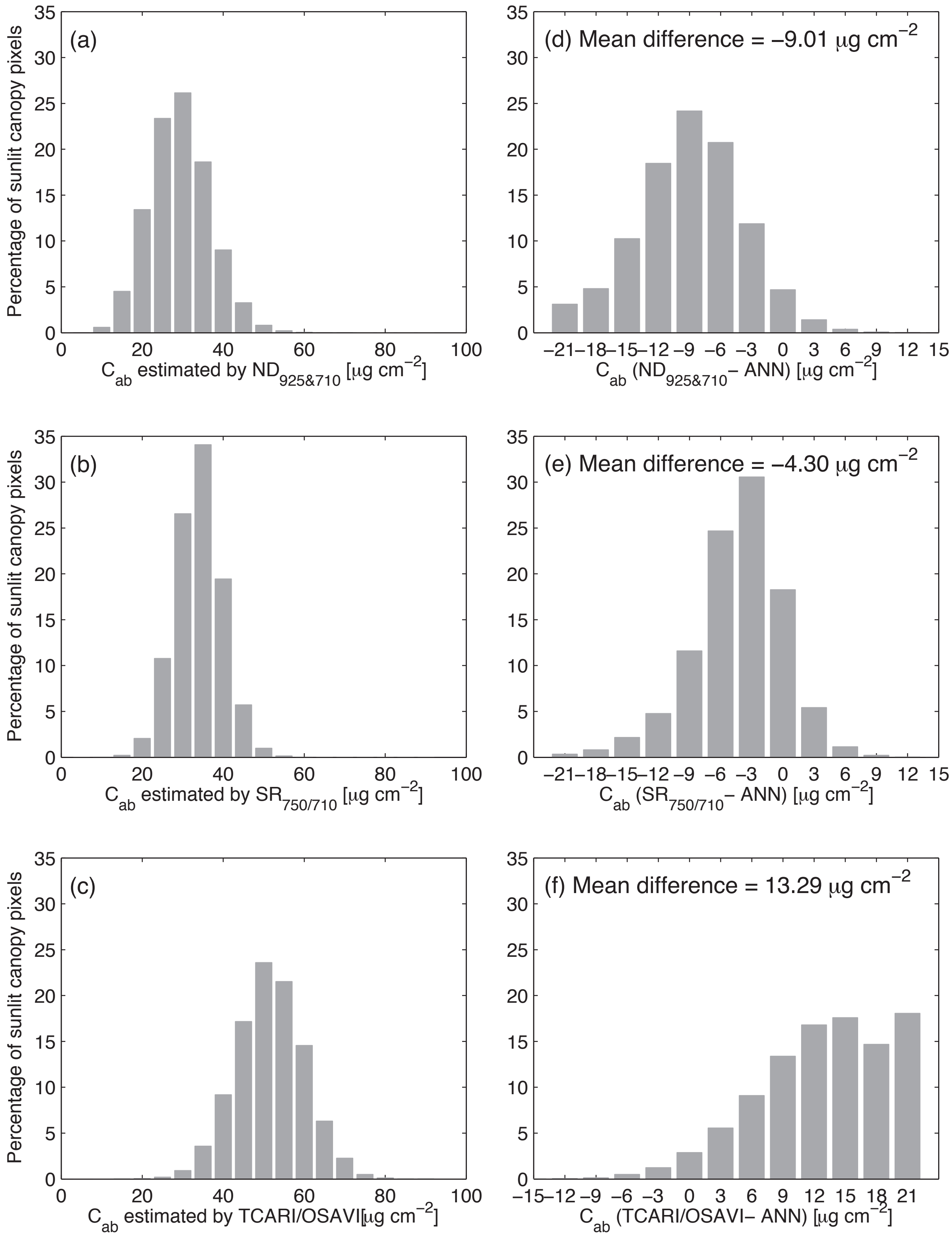

Fig. 8. Histograms showing the percentage of sunlit crown pixels per C_{ab} value estimated by the Normalized Difference between reflectance at 925 and 710 nm ($ND_{925\&710}$) (a), Simple reflectance Ratio between 750 and 710 nm ($SR_{750/710}$) (b) and ratio TCARI/OSAVI (c), and the distribution of estimated C_{ab} differences computed between all three optical indices and the ANN (d, e, f).

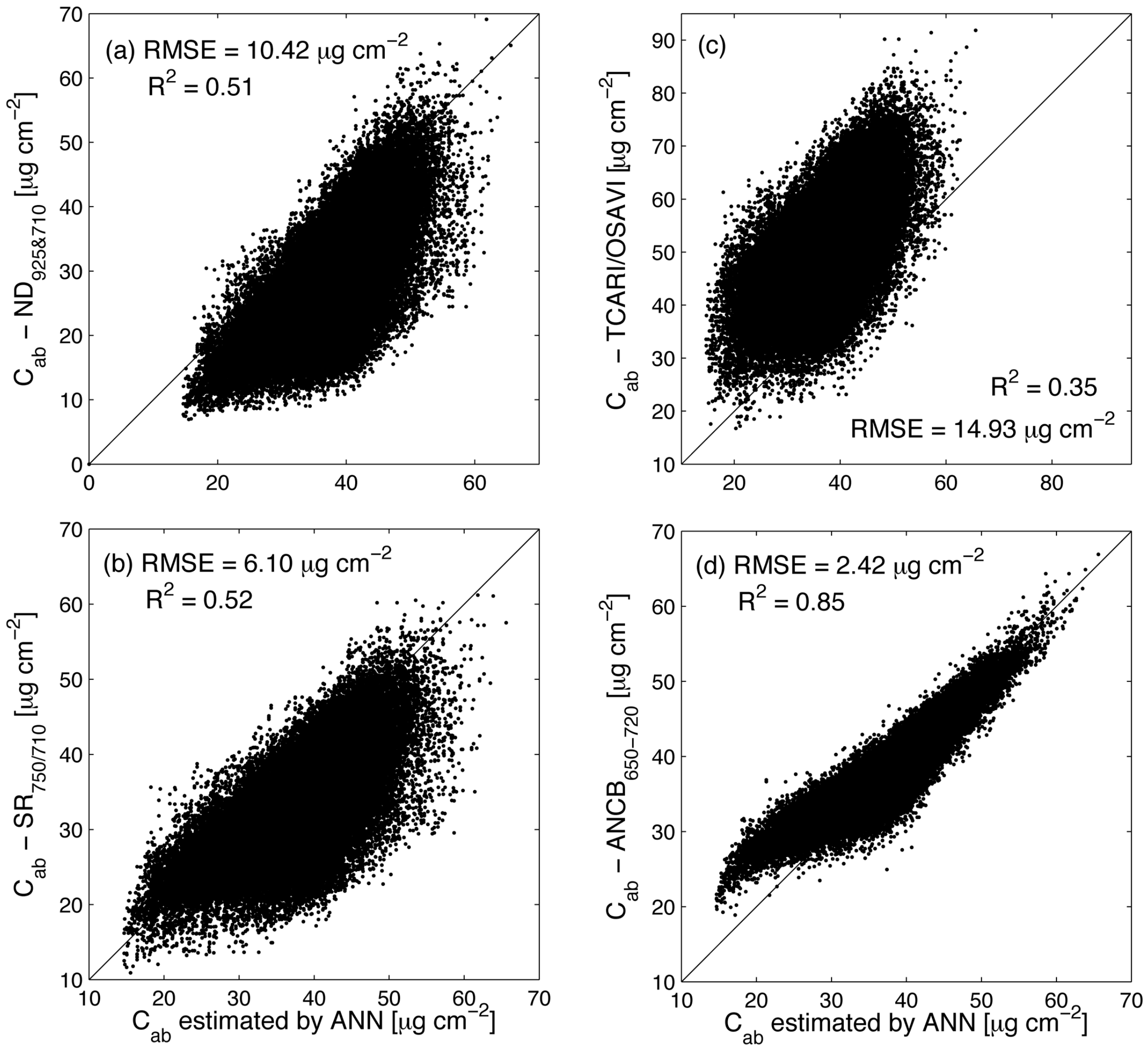

Fig. 9. Scatterplot of leaf chlorophyll content (C_{ab}) retrieved by artificial neural network (ANN) plotted against the C_{ab} estimates of Normalized Difference ($ND_{925\&710}$) (a), Simple reflectance Ratio ($SR_{750/710}$) (b), ratio of TCARI/OSAVI indices (c) and $ANCB_{650\text{-}720}$ optical index (d). Each dot symbol represents one pixel of a sunlit tree crown identified in the AISA Eagle image of the test site (R^2 ~ coefficient of determination, RMSE ~ root mean square error).

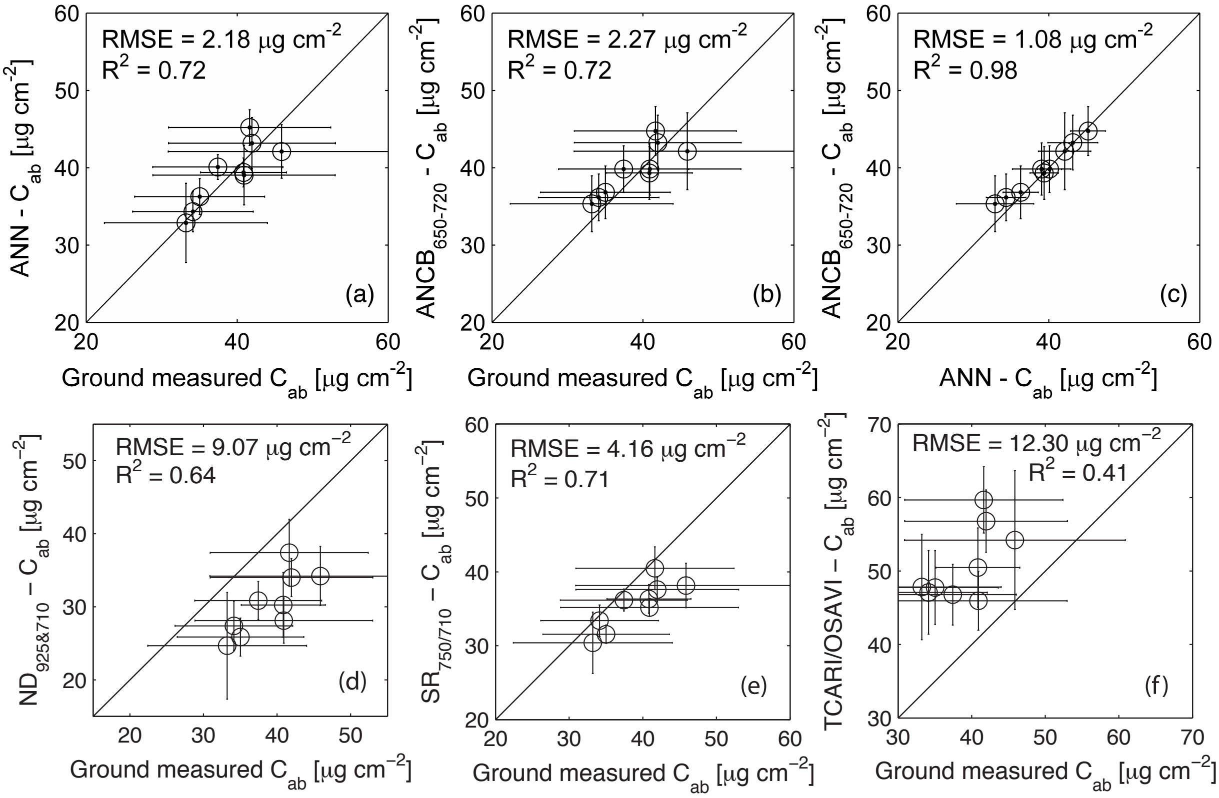

Fig. 10. Validation of leaf chlorophyll content (C_{ab}) retrieved for the sampled spruce crowns from the AISA Eagle image using artificial neural network (ANN) (a), $ANCB_{650\text{-}720}$ optical index (b), Normalized Difference between reflectance at 925 and 710 nm ($ND_{925\&710}$) (d), Simple reflectance Ratio between 750 and 710 nm ($SR_{750/710}$) (e), ratio TCARI/OSAVI (f) and the reciprocal comparison of ANN and $ANCB_{650\text{-}720}$ estimations (c). Each circle represents one tree crown, horizontal bars represent two standard deviations of C_{ab} values either measured on the ground or retrieved by ANN and optical indices. (R^2 ~ coefficient of determination, RMSE ~ root mean square error).

Appendix A: Chlorophyll sensitivity of ANCB$_{650\text{-}720}$ and three other optical indices in the case of broadleaf canopies

To compare the C_{ab} sensitivity of the newly proposed ANCB$_{650\text{-}720}$ and three previously published optical indices also in a case of broadleaf plants, we simulated a top-of-the-canopy bi-directional reflectance factor (BRF) of two structurally different broadleaf canopies: i) a homogeneous grassland (scenario SC1) and ii) a heterogeneous deciduous forest (scenario SC2). The simulations were performed using the radiative transfer models PROSPECT-4 (Feret et al., 2008) and DART (Gastellu-Etchegorry et al., 2004). The sun-sensor geometry of the broadleaf simulations was kept as for the Norway spruce simulations, i.e. sun zenith angle equal to 47.8° and sun azimuth angle equal to 183.4°. Only the canopy reflectance observed from nadir was considered in this sensitivity test. We simulated canopy BRF at 11 discrete wavelengths corresponding to the AISA Eagle spectral bands with the following central wavelengths: 551, 652, 661, 670, 680, 689, 708, 717, 745, and 802 nm (full width half maximum of 10 nm).

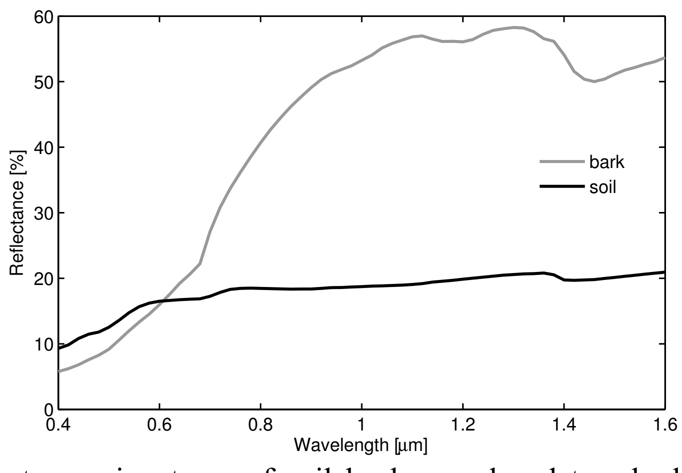

Fig. A1. Reflectance signatures of soil background and tree bark as used in PROSPECT-DART radiative transfer simulations of broadleaf canopy scenarios (SC1 and SC2).

The optical properties of the soil background and woody materials were measured during the field campaign at Bílý Kříž test site in the ASD integrating sphere coupled with the ASD FieldSpec PRO spectroradiometer (ASD, Inc., USA); their spectral signatures are shown in

Fig. A1. The leaf optical properties were simulated with the PROSPECT model (version 4). The input parameters are summarized in Table A1. The variable of interest C_{ab} was kept free, ranging between 10 and 85 μg cm^{-2} increasing with a step of 15 μg cm^{-2}. In total, 216 different combinations of structurally simple 1-D homogeneous turbid medium of grassland canopy were simulated within scenario SC1 by varying the leaf chlorophyll content (C_{ab}), leaf area index (LAI) and leaf angle distribution (LAD). Scenario SC2, representing a structurally heterogeneous 3-D canopy of a mixed deciduous forest, was constructed from two horizontal leaf layers: i) the understory layer modeled as small spherical bushes and ii) the overstory layer modeled as ellipsoidal crowns with woody trunks. We executed 108 different canopy realizations of SC2 by varying the input parameters C_{ab}, LAI and canopy cover. An overview of fixed and varying input parameters for both scenarios is provided in Table A1. All four chlorophyll sensitive optical indices ($ANCB_{650-720}$, $ND_{925\&710}$, $SR_{750/710}$ and TCARI/OSAVI) were computed from the simulated canopy BRF (in case of SC2 only from sunlit crown pixels) and plotted against C_{ab} to investigate their relationship.

The dependency of $AUC_{650-720}$ and CBD_{670} on C_{ab} is for both scenarios very similar to Norway spruce crowns (Fig. 5a and 5b) and also empirical relations between the indices and C_{ab} are statistically significant (Fig. A2 and A3). However, a large variability in computed values of $ND_{925\&710}$ and $SR_{750/710}$ is seen in the case of SC1. Since this variability is not observed for SC2, it is logically caused by six different leaf angle distributions. $ANCB_{650-720}$ and TCARI/OSAVI are less influenced by the changing leaf angle distribution, varying mainly for C_{ab} lower than 40 μg cm^{-2}. For both scenarios, $ANCB_{650-720}$ showed the strongest C_{ab} predictive power (R^2 = 0.95 and 0.99, p < 0.01 and 0.001) described by a linear function. However, $ANCB_{650-720}$ predictions for C_{ab} values below 20 μg cm^{-2} are for both broadleaf canopies less reliable than those of Norway spruce crowns (Fig. A2c and A3c).

Table A1: Key input parameters of the PROSPECT-DART radiative transfer simulations conducted for sensitivity analyses of chlorophyll estimating indices for two broadleaf canopies: grassland (SC1) and deciduous forest (SC2). (NA ~ not applicable).

Parameters	Units	SC1 (grassland)	SC2 (deciduous forest)	
			Bushes	Trees
Leaf level (PROSPECT)				
Chlorophyll content	[μg cm^{-2}]	10, 25, 40, 55, 70, 85	10, 25, 40, 55, 70, 85	
Water content	[g cm^{-2}]	0.0175	0.0199	0.0199
Leaf mass per area	[g cm^{-2}]	0.0084	0.0043	0.0066
Structural parameter N	[-]	1.75	1.83	2.66
Canopy level (DART)				
Canopy height	[m]	0.5 ± 0.15	1.5 ± 0.2	8.0 ± 1.5
Crown shape		NA	Spherical	Ellipsoidal
Trunk diameter	[m]	NA	NA	0.15
Proportion of leaf cells	[%]	100	80	60
Leaf angle distribution	[-]	Erectophile, Spherical, Planophile, Uniform, Extremophile Plagiophile	Spherical	Planophile
Leaf area index	[-]	1, 2, 3, 4, 5, 6	4, 5, 6, 7, 8, 9	
Canopy cover	[%]	100	45, 65, 85	

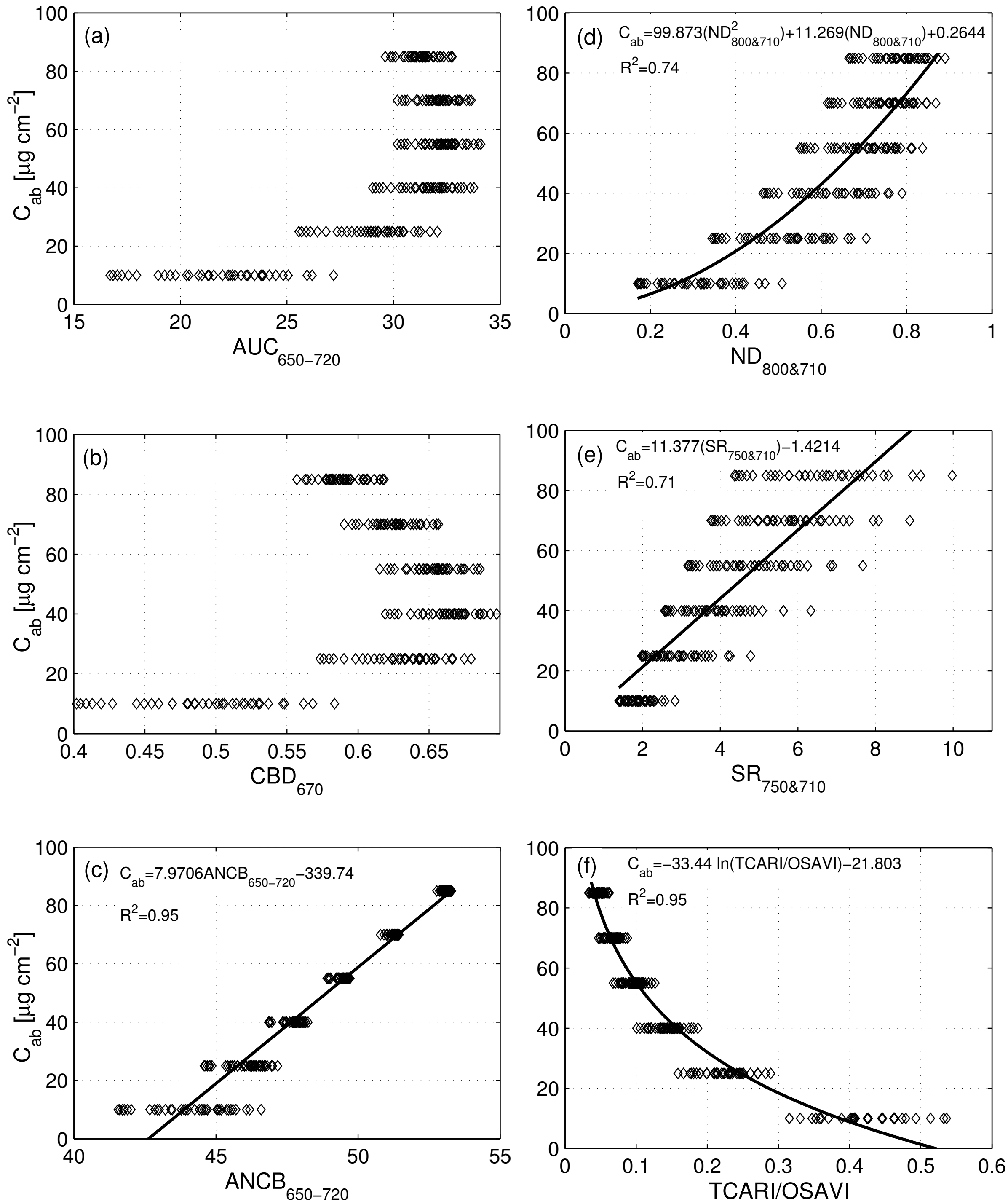

Fig. A2. Relationship between leaf chlorophyll content (C_{ab}) and the Area Under Curve ($AUC_{650\text{-}720}$) of continuum removed reflectance between 650-720 nm (a), Continuum Band Depth at 670 nm (CBD_{670}) (b), $ANCB_{650\text{-}720}$ optical index (c), Normalized Difference ($ND_{925\&710}$) (d), Simple reflectance Ratio ($SR_{750/710}$) (e) and ratio of TCARI/OSAVI indices (f) computed from PROSPECT-DART radiative transfer simulations for homogeneous grassland (scenario SC1). (R^2 ~ coefficient of determination of the best fitting mathematical function).

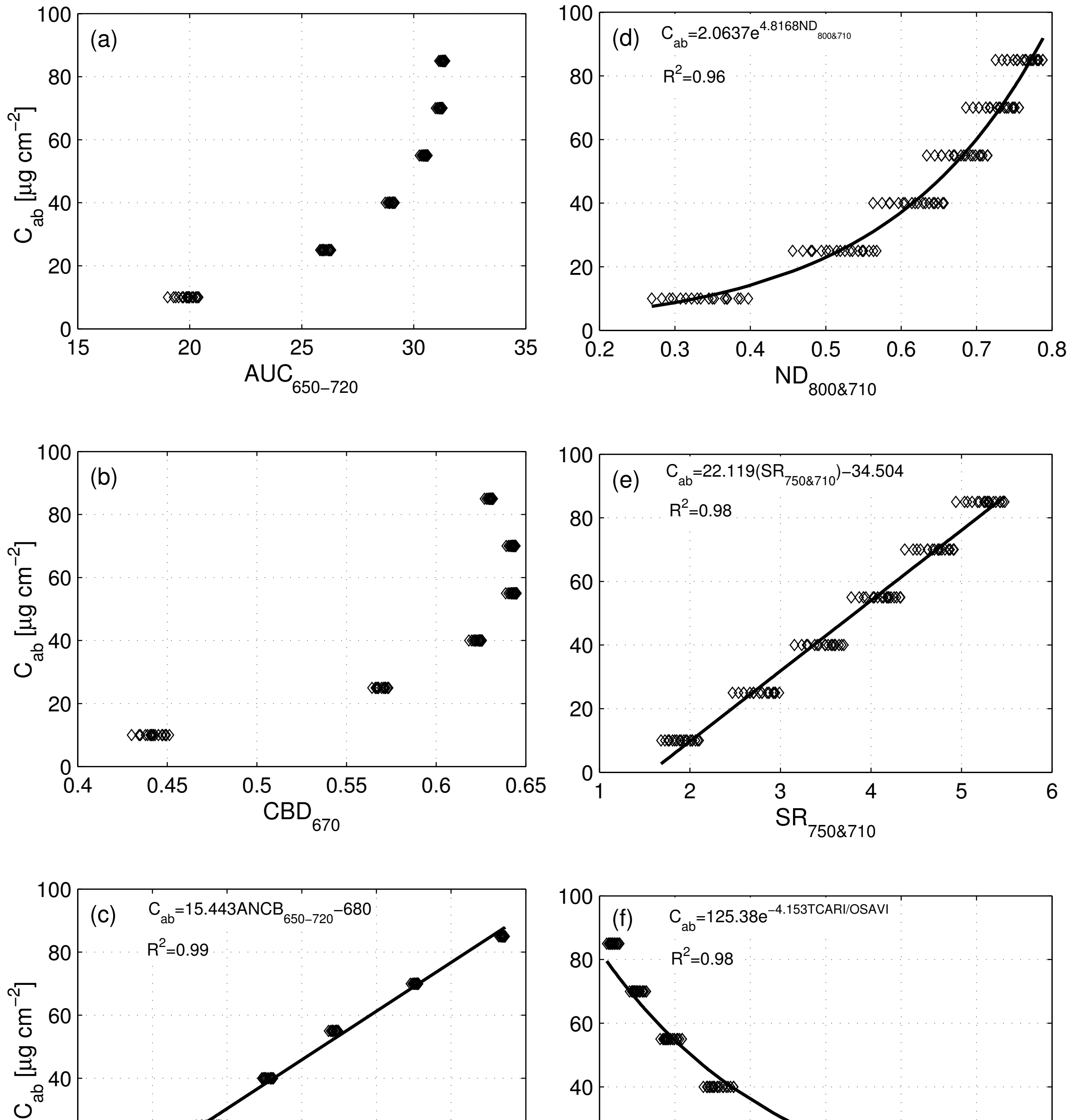

Figure A3. Relationship between leaf chlorophyll content (C_{ab}) and the Area Under Curve ($AUC_{650-720}$) of continuum removed reflectance between 650-720 nm (a), Continuum Band Depth at 670 nm (CBD_{670}) (b), $ANCB_{650-720}$ optical index (c), Normalized Difference ($ND_{925\&710}$) (d), Simple reflectance Ratio ($SR_{750/710}$) (e) and ratio of TCARI/OSAVI indices (f) computed from sunlit crown pixels simulated by PROSPECT-DART radiative transfer for a heterogeneous deciduous forest stand (scenario SC2). (R^2 ~ coefficient of determination of the best fitting mathematical function).

References:

Feret, J.B., Francois, C., Asner, G.P., Gitelson, A.A., Martin, R.E., Bidel, L.P.R., Ustin, S.L., le Maire, G., & Jacquemoud, S. (2008). PROSPECT-4 and 5: Advances in the leaf

optical properties model separating photosynthetic pigments. *Remote Sensing of Environment*, 112, 3030-3043.
Gastellu-Etchegorry, J.P., Martin, E., & Gascon, F. (2004). DART: a 3D model for simulating satellite images and studying surface radiation budget. *International Journal of Remote Sensing*, 25, 73-96.

Appendix B: Comparison of the $ANCB_{650-720}$ – C_{ab} relationship for sunlit and shaded spruce crown parts simulated with PROSPECT and DART

Similarly to the structurally heterogeneous 3-D canopy of a mixed deciduous forest (Appendix A), 108 Norway spruce scenes parameterized according to Table 1 and Table 2 were simulated with spruce-adapted PROSPECT and DART models for a leaf chlorophyll content varying between 10 and 85 μg cm^{-2} increasing with a step of 15 μg cm^{-2}. Pixels of sunlit and shaded crown parts were separated using a maximum likelihood classification. $AUC_{650-720}$, CBD_{670} and $ANCB_{650-720}$ were computed from the top-of-the-canopy bi-directional reflectance factor (BRF) averaged per simulation and plotted against the predefined C_{ab} classes to investigate potential differences in C_{ab} empirical relationships for sunlit and shaded pixels. Fig. B1 demonstrates that the $AUC_{650-720}$ and CBD_{670} values of shaded crown parts vary more than those of sunlit parts. $ANCB_{650-720}$ is, nevertheless, reducing this variability and producing the statistically significant exponential relationship ($R^2 = 0.99$, $p < 0.001$) of very similar shape as for sunlit parts (Fig. B1c). Based on this result, one could propose to use the whole spruce crowns for C_{ab} estimation regardless their sunlit or shaded appearance. It is, however, important to stress out that the presented relationships were obtained from the radiative transfer modeling of a generalized spruce forest stand, which omitted any kind of image noise. Depending on radiometric specifications of an airborne sensor, the reflectance signal of shaded pixels may contain a higher portion of a random noise. The presence of noise, the spatially specific forest canopy shade intensity, and importantly the limited reflectance dynamic range (Fig. 3 indicates that reflectance of shaded pixels is twice lower than of sunlit crown pixels) will predominantly result in C_{ab} estimates of low accuracy.

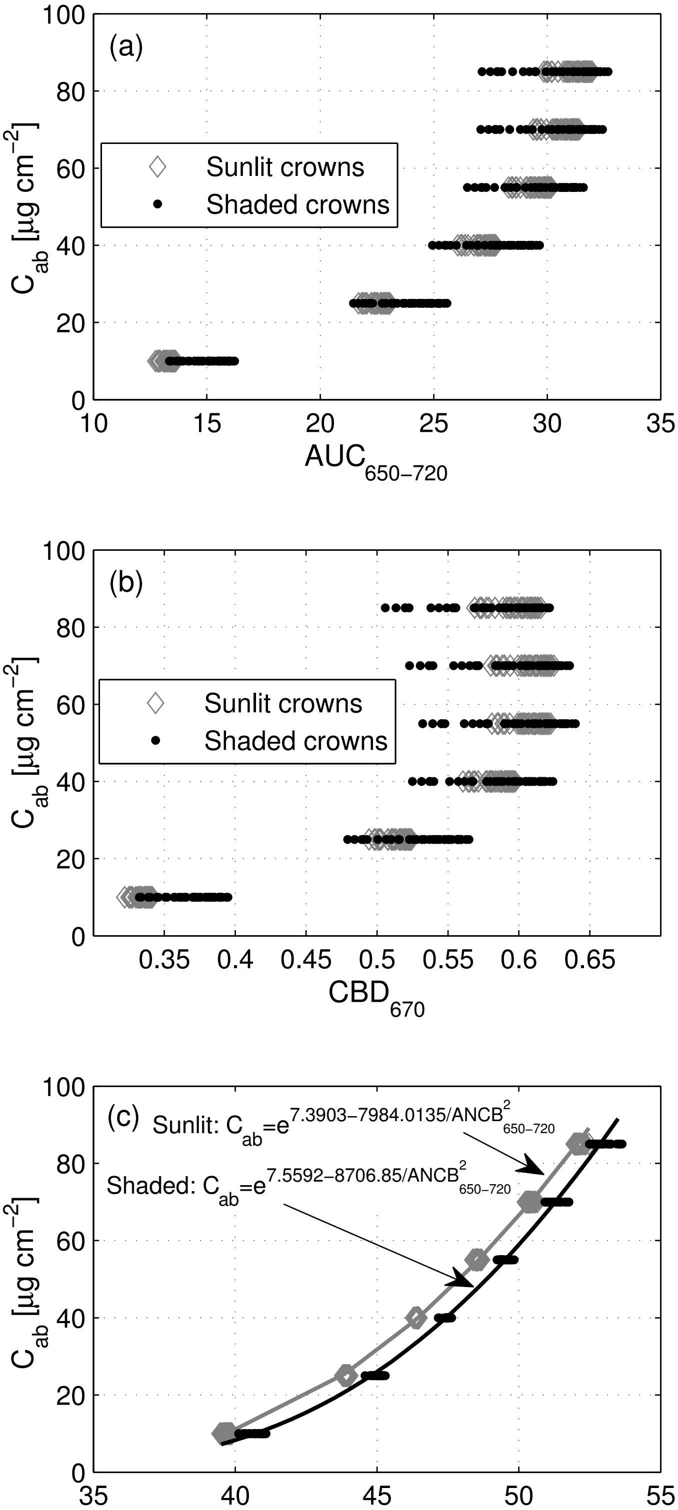

Fig. B1. The $ANCB_{650\text{-}720}$ optical index (c) computed from the Area Under Curve ($AUC_{650\text{-}720}$) of continuum-removed reflectance (a) and Continuum Band Depth at 670 nm (CBD_{670}) (b) separately for sunlit and shaded Norway spruce crown pixels. The equations represent the best fitting exponential functions (coefficient of determination R^2 = 0.99, significance probability level p < 0.001). A single diamond/dot symbol represents one of the PROSPECT-DART simulated leaf area index (LAI) values (LAI ~ <4, 9> with a step of 1) within three predefined canopy closures (CC ~ 75, 85 and 95%).